Antibody-lectin chimeras for glyco-immune checkpoint blockade

Jessica C. Stark[1,2,*], Melissa A. Gray[1,*], Simon Wisnovsky[3], Itziar Ibarlucea-Benitez[4], Marta Lustig[5], Nicholas M. Riley[1], Mikaela K. Ribi[1], Wesley J. Errington[6], Bence Bruncsics[7], Casim A. Sarkar[6], Thomas Valerius[5], Jeffrey V. Ravetch[4], Carolyn R. Bertozzi[1,8]

[1]Department of Chemistry and Sarafan ChEM-H, Stanford University, Stanford, CA, USA

[2]Current affiliation: Department of Biological Engineering, Department of Chemical Engineering, and Koch Institute for Integrative Cancer Research, Massachusetts Institute of Technology, Cambridge, MA, USA

[3]Faculty of Pharmaceutical Sciences, University of British Columbia, Vancouver, BC, Canada

[4]Laboratory of Molecular Genetics and Immunology, The Rockefeller University, New York, NY, USA

[5]Division of Stem Cell Transplantation and Immunotherapy, Department of Medicine II, Christian Albrechts University Kiel and University Medical Center Schleswig-Holstein, Kiel, Germany

[6]Department of Biomedical Engineering, University of Minnesota, Minneapolis, MN, USA

[7]Department of Measurement and Information Systems, Budapest University of Technology and Economics, Budapest, Hungary

[8]Howard Hughes Medical Institute, Stanford, CA, USA

[*]J.C.S. and M.A.G. contributed equally

Abstract

Despite the curative potential of checkpoint blockade immunotherapy, most patients remain unresponsive to existing treatments. Glyco-immune checkpoints – interactions of cell-surface glycans with lectin, or glycan-binding, immunoreceptors – have emerged as prominent mechanisms of immune evasion and therapeutic resistance in cancer. Here, we describe antibody-lectin chimeras (AbLecs), a modular platform for glyco-immune checkpoint blockade. AbLecs are bispecific antibody-like molecules comprising a cell-targeting antibody domain and a lectin "decoy receptor" domain that directly binds glycans and blocks their ability to engage inhibitory lectin receptors. AbLecs potentiate anticancer immune responses including phagocytosis and cytotoxicity, outperforming most existing therapies and combinations tested. By targeting a distinct axis of immunological regulation, AbLecs synergize with blockade of established immune checkpoints. AbLecs can be readily designed to target numerous tumor and immune cell subsets as well as glyco-immune checkpoints, and therefore represent a new modality for cancer immunotherapy.

Main

T cell checkpoint blockade immunotherapies (e.g., PD-1/PD-L1 or CTLA-4 targeting antibodies) are now used to treat nearly half of all cancer patients in the US[1]. However, these therapies are effective in only a small fraction (<20%) of treated patients across cancer types[1] and, of those who respond, at least 25% will develop resistance[2]. Thus, there is an urgent need for therapies targeting additional immune checkpoints that drive cancer progression.

Altered cell surface glycosylation is a hallmark of cancer that is associated with poor disease prognosis[3–5]. These altered glycan structures modulate immune cell function through interactions with lectin (glycan-binding) immunoreceptors, including sialic acid-binding immunoglobulin-like lectins (Siglecs)[6], selectins[7], and galectins[8,9]. In particular, multiple recent

45 studies indicate that upregulation of cell-surface sialoglycans allows tumors to engage inhibitory
46 Siglec receptors on immune cells and evade immune surveillance[10–27]. Taken together, glyco-
47 immune checkpoints are emerging as attractive targets for cancer immunotherapy.

48 However, multiple challenges have historically prevented therapeutic targeting of glyco-
49 immune checkpoints in cancer (**Fig 1a**). The weak immunogenicity of mammalian glycan
50 structures can undermine the development of specific and high-affinity anti-glycan antibodies. To
51 put this in perspective, a recent report cataloged 417 commercially available antibodies targeting
52 glycans[28]. The same study noted that a single supplier offers 287 unique antibodies to tubulin and
53 269 unique antibodies to CD4, meaning that there are more antibodies to these two proteins
54 available from a single supplier than all the commercially available anti-glycan antibodies
55 combined. Further complicating monoclonal antibody development is the fact that many lectin
56 receptors have multiple ligands that are expressed in the context of cancer[10,15,17,23,29], and often
57 the precise identities of their ligands are unknown. "Decoy receptor" molecules composed of a
58 lectin glycan-binding domain fused to an antibody Fc domain address this complexity by retaining
59 native glycan-binding specificities; however, their low binding affinities (typically with K_Ds in the
60 μM to mM range[30]) preclude their use as therapeutics.

61 We recently developed enzyme conjugates for targeted degradation of glycans[12,16] or
62 glycoproteins[31] as an alternative approach to potentiate anti-tumor immunity, but these molecules
63 require substantial engineering of enzyme kinetics in order to target new types of glycans. In
64 addition, such approaches are currently restricted to degradation of broad classes of glycans
65 (e.g., sialoglycans[12,16]) or glycoproteins (e.g., mucins[31]), rather than the specific molecules
66 involved in immune regulation. Finally, while lectin-targeted blockade antibodies such as those
67 directed against galectin-9[32] and Siglec-15[33] as well as a sialidase-Fc fusion for sialoglycan
68 degradation[34] are being tested in the clinic, these untargeted checkpoint blockade reagents could
69 elicit immune-related adverse events, which are observed in at least 50% of patients treated with
70 existing checkpoint blockade immunotherapies[35]. In contrast, targeted immunotherapies (e.g.,

71 monoclonal antibodies targeting tumor-associated antigens) generally offer more favorable safety
72 profiles[36]. Overall, our inability to specifically and directly block immunomodulatory glycans, even
73 after development of multiple therapeutic modalities, highlights the significance of this
74 technological gap.

75 Here, we describe antibody-lectin (AbLec) chimeras as a modular platform to target
76 glycans for cancer immunotherapy. AbLecs couple glycan binding domains from lectin receptors
77 to antibodies directed against an antigen on the target cell surface (**Fig. 1a**). This approach
78 uniquely enables blockade of immunomodulatory glycans at nanomolar concentrations agnostic
79 of their specific identities. We demonstrate proof-of-concept of the AbLec platform through the
80 development and characterization of AbLecs combining tumor-targeting antibodies with decoy
81 receptor domains from Siglecs-7 and -9, which have been shown to mediate immune suppression
82 in multiple cancers[11–13,16–27]. We show that tumor-targeting AbLecs enhance antibody-dependent
83 phagocytosis and cytotoxicity of cancer cells by multiple primary immune cell subsets compared
84 to the parent monoclonal antibody. AbLecs outperformed combination of a tumor-targeting
85 antibody and a lectin receptor-blocking antibody, suggesting there is a therapeutic benefit gained
86 by targeting glycans directly. We show that the AbLec platform can be applied to target diverse
87 tumor-associated antigens, including HER2, CD20, and EGFR, and cancer cells with varying
88 levels of antigen expression. Further, we designed and validated dual blockade AbLecs that
89 simultaneously block protein-based immune checkpoints (e.g., PD-1/PD-L1, CD47/SIRPα) as
90 well as glyco-immune checkpoints known to play roles in cancer (e.g., Siglec-7[13,15,19,20,25], galectin-
91 9[37,38]). We found that glyco-immune checkpoint blockade was synergistic with blockade of these
92 established checkpoints. These results indicate that AbLecs target a non-redundant axis of
93 immune suppression in cancer and could expand the subset of patients who respond to
94 immunotherapy. In sum, AbLecs represent a generalizable approach for glyco-immune
95 checkpoint blockade and a new modality for cancer immunotherapy.
96

97 ## Results

98 *AbLecs bind to targeted cells at nanomolar concentrations*

99 We hypothesized that high-affinity binding of an antibody Fab domain to tumor antigens
100 would allow AbLecs to accumulate at sufficiently high local concentrations to permit binding of a
101 relatively low affinity lectin domain to inhibitory glycans on the same cell. As proof-of-concept, we
102 created AbLecs that combine the Fab domain from trastuzumab, an FDA-approved monoclonal
103 antibody that binds the tumor antigen HER2, with the extracellular domains of Siglec-7 or -9 fused
104 to an Fc domain. We used a modified knobs-into-holes Fc engineering approach[39] to facilitate
105 self-assembly of heterotrimeric AbLecs in a single expression culture (**Fig. 1b**). Indeed,
106 coexpression of trastuzumab heavy and light chains with Siglec-7-Fc or Siglec-9-Fc in Expi293
107 cells resulted in expression of predominant protein species with molecular weights consistent with
108 heterotrimeric AbLecs (**Fig. 1c**). Reducing SDS-PAGE analysis of purified proteins showed that
109 trastuzumab x Siglec-7 (T7) and trastuzumab x Siglec-9 (T9) AbLecs were composed of 3
110 disulfide bonded protein chains consistent with the molecular weights of the Siglec-Fc and the
111 trastuzumab heavy and light chains (**Fig. 1c**). Western blotting against HA and 6xHis tags on the
112 Siglec-Fc and antibody heavy chains, respectively, further demonstrated that full-length AbLecs
113 are composed of both antibody and decoy receptor arms (**Fig. 1d**), which was confirmed by mass
114 spectrometry (**Extended Data Fig. 1**).

115 We next characterized binding of T7 and T9 AbLecs to HER2+ cell lines compared to
116 trastuzumab and Siglec-Fc decoy receptor controls. Dissociation constant (K_D) values for T7 and
117 T9 AbLecs were measured by quantifying binding to SK-BR-3 cells at various concentrations via
118 flow cytometry. SK-BR-3 cells express the HER2 antigen bound by trastuzumab as well as ligands
119 for Siglecs-7 and -9 (Sig7/9L) (**Fig. 1e**). As expected, the decoy receptor controls (Siglec-7/9-Fc)
120 bind only at low levels to SK-BR-3 cells, even at the highest concentrations tested (200 nM),
121 despite the fact that SK-BR-3 cells express Siglec-7 and -9 ligands (**Fig. 1f**). However, by

122 combining the decoy receptor arm with the high affinity trastuzumab antibody arm, AbLecs bind
123 to SK-BR-3 cells with K_D values in the low nM range, similar to that of the parent bivalent antibody
124 trastuzumab (**Fig. 1f, g**). Thus, AbLecs enable recruitment of otherwise low affinity lectin binding
125 domains to cell surfaces at nanomolar concentrations.

126 Despite the low affinity of the Siglec domain in comparison to the antibody arm, AbLec
127 binding affinity is influenced by both components. By mutating a conserved arginine residue in
128 the Siglec-Fc binding site to an alanine, we created T7A and T9A AbLec mutants that are reported
129 to exhibit significantly reduced affinities for Siglec ligands[40]. Arginine mutant AbLecs exhibited
130 reduced binding to SK-BR-3 cells, measured by a ~2-3-fold increase in apparent K_D compared to
131 WT AbLecs (**Extended Data Fig. 2a-c**).

132 We further interrogated the mechanism of AbLec binding via a structure-guided
133 computational modeling approach[41]. We used the recently developed *MVsim* toolset[42] to construct
134 a computational model of T7 AbLec binding trained using our experimental data (**Extended Data**
135 **Fig. 2d**). Our computational model estimated that the apparent concentration of Siglec-7 ligands
136 on the cancer cell surface was >2 orders of magnitude higher than that of the HER2 antigen
137 (**Extended Data Fig. 2e**; $[HER2]_{app}$ = 0.2 μM; $[Sig7L]_{app}$ = 27 μM), suggesting that the abundance
138 of accessible glycan ligands offsets the low monovalent Siglec domain affinity and facilitates
139 cooperative AbLec binding. This observed contribution of the Siglec-Fc arm to binding may
140 explain why AbLec dissociation constants are of the same order of magnitude as the bivalent
141 parent antibody trastuzumab, despite having only one antibody arm.
142

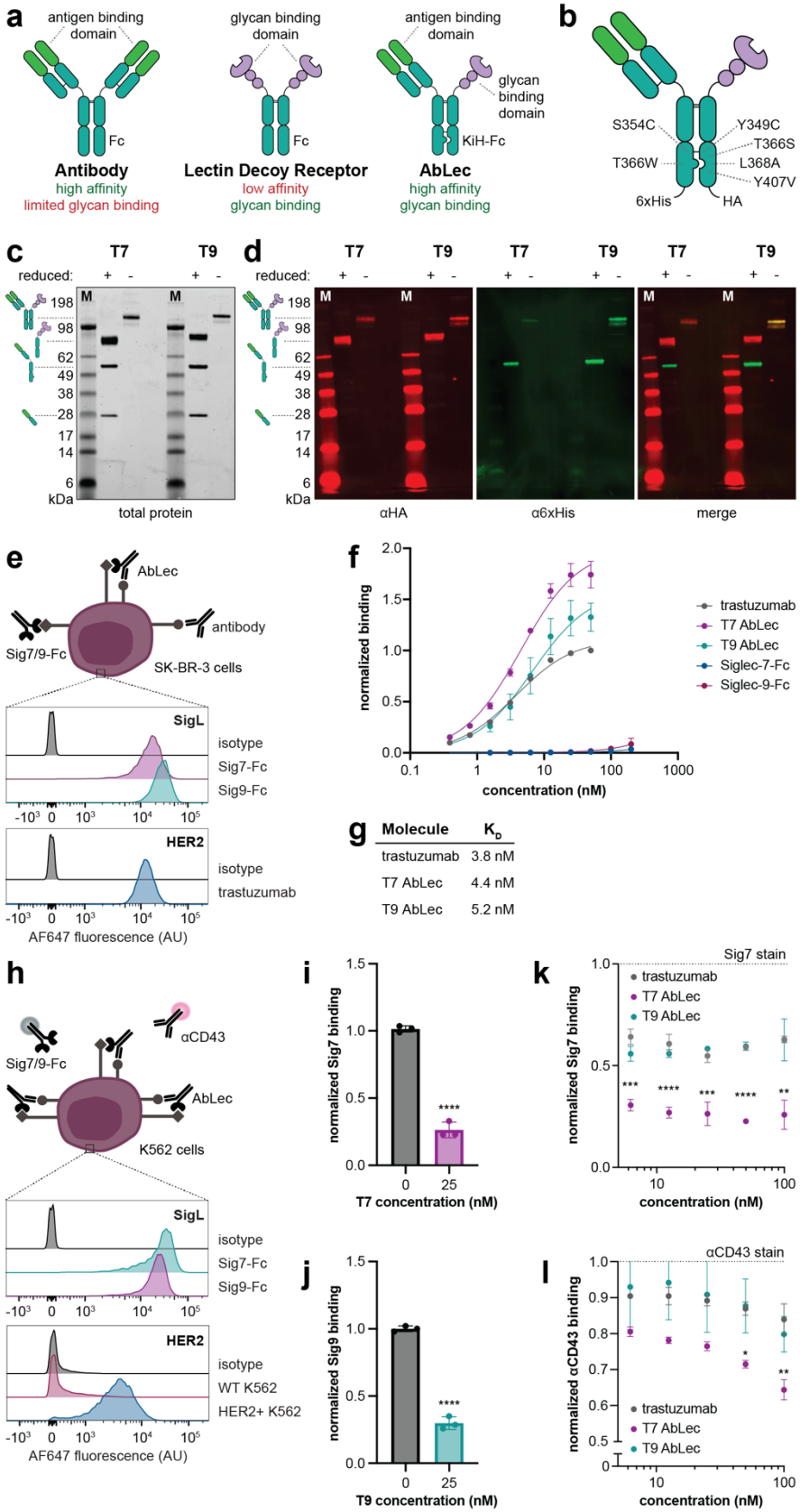
a
antigen binding domain
Fc
Antibody
high affinity
limited glycan binding
glycan binding domain
Fc
Lectin Decoy Receptor
low affinity
glycan binding
antigen binding domain
glycan binding domain
KiH-Fc
AbLec
high affinity
glycan binding
b
S354C
Y349C
T366S
T366W
L368A
Y407V
6xHis
HA
c
T7
T9
reduced:
198
98
62
49
38
28
17
14
6
kDa
total protein
d
αHA
α6xHis
merge
e
AbLec
antibody
Sig7/9-Fc
SK-BR-3 cells
SigL
isotype
Sig7-Fc
Sig9-Fc
HER2
isotype
trastuzumab
AF647 fluorescence (AU)
f
normalized binding
concentration (nM)
trastuzumab
T7 AbLec
T9 AbLec
Siglec-7-Fc
Siglec-9-Fc
g
Molecule
K_D
trastuzumab 3.8 nM
T7 AbLec 4.4 nM
T9 AbLec 5.2 nM
h
αCD43
Sig7/9-Fc
AbLec
K562 cells
SigL
isotype
Sig7-Fc
Sig9-Fc
HER2
isotype
WT K562
HER2+ K562
AF647 fluorescence (AU)
i
normalized Sig7 binding
T7 concentration (nM)
j
normalized Sig9 binding
T9 concentration (nM)
k
Sig7 stain
normalized Sig7 binding
concentration (nM)
trastuzumab
T7 AbLec
T9 AbLec
l
αCD43 stain
normalized αCD43 binding
concentration (nM)
trastuzumab
T7 AbLec
T9 AbLec

143

144 **Figure 1. AbLecs enable the use of lectin decoy receptors for glyco-immune checkpoint blockade.**

145 (**a**) AbLecs couple tumor-targeting antibodies to glycan binding domains from lectin immunoreceptors,
146 enabling blockade of immunosuppressive glycans at therapeutically relevant concentrations.

147 (**b**) Fc engineering in a human IgG1 antibody framework facilitates self-assembly of AbLecs.

148 (**c**) Total protein stain of SDS-PAGE of purified T7 and T9 AbLecs under disulfide-reducing and non-
149 reducing conditions. Gel is representative of n = 3 replicates.

150 (**d**) Western blot detection of antibody heavy chain (α6xHis) and Siglec-Fc chains (αHA) revealed that
151 AbLecs are composed of antibody and Siglec decoy receptor arms. Blots are representative of n = 3
152 replicates.

153 (**e**) SK-BR-3 cells express the HER2 antigen bound by trastuzumab as well as ligands for Siglec-7 and -9
154 (Sig7L and Sig9L, respectively) as measured by Siglec-Fc binding and analyzed via flow cytometry.
155 Histograms are representative of n = 3 biological replicates (quantified in **Extended Data Fig. 2c-d**).

156 (**f**) Binding of T7 AbLec, T9 AbLec, trastuzumab, Siglec-7-Fc, and Siglec-9-Fc to SK-BR-3 cells was
157 quantified via flow cytometry. Data are mean ± standard deviations (s.d.) of n = 3 biological replicates,
158 normalized to staining with 50 nM trastuzumab for each replicate.

159 (**g**) Dissociation constants for trastuzumab, T7, and T9 AbLecs determined by fitting experimental data
160 from (**f**) to a one-site total binding curve.

161 (**h**) HER2+ K562 cells express the HER2 antigen as well as Sig7L and Sig9L via flow cytometry.
162 Histograms are representative of n = 3 biological replicates (quantified in **Extended Data Fig. 2c-d**).

163 (**i, j**) T7 (**i**) or T9 (**j**) AbLec treatment blocks Siglec-7 or Siglec-9 receptor binding, respectively, in
164 competitive binding assays with dye labeled Siglec-7/9-Fc. Data are mean ± s.d. of n = 3 biological
165 replicates, normalized to Siglec-Fc staining without AbLec.

166 (**k**) T7 AbLec, but not trastuzumab or T9 AbLec, blocks Siglec-7 receptor binding in competitive binding
167 assays with dye labeled Siglec-7-Fc. Data are mean ± s.d. of n = 3 biological replicates, normalized to
168 Siglec-7-Fc staining with 0 nM AbLec or antibody.

169 (**l**) Detection of αCD43 antibody (MEM-59) binding in competitive binding assays with increasing
170 concentrations of T7 AbLec, T9 Ablec, or trastuzumab. The MEM-59 antibody binds to the same epitope
171 on CD43 recognized by the Siglec-7 receptor. Data are mean ± s.d. of n = 3 biological replicates,
172 normalized to αCD43 staining without AbLec or antibody.

173

174 *AbLecs selectively block lectin receptor binding epitopes*

175 We next asked whether AbLecs could successfully block engagement of their targeted
176 glycan ligands by competing with lectin receptors. Toward this end, we tested the ability of T7 and
177 T9 AbLecs to compete with fluorescently-labeled Siglec decoy receptors for binding to HER2+
178 K562 cells. This cell line expresses a higher ratio of Sig7L and Sig9L to the targeted antigen
179 HER2, offering a more challenging target for glycan blockade (**Fig. 1h**). Both T7 and T9 AbLecs
180 bound to HER2+ K562 cells with low nanomolar K_D values (**Extended Data Fig. 2f, g**). Treatment
181 of cells with T7 or T9 AbLec significantly reduced binding of fluorescently labeled Siglec-7 or

182 Siglec-9, respectively, by flow cytometry (**Fig. 1i, j**). Importantly, AbLec binding to target cells is
183 not cytotoxic: we did not observe any defects in SK-BR-3 or HER2+ K562 cell growth over 72
184 hours following AbLec treatment (**Extended Data Fig. 2h-k**). AbLecs further selectively block
185 binding of the targeted lectin. Treatment with the T7 AbLec blocked binding of the cognate Siglec-
186 7 decoy receptor to a greater extent than trastuzumab or the non-cognate T9 AbLec at all
187 concentrations tested (**Fig. 1k**).

188 We wanted to test whether AbLecs block the same epitopes bound by their cognate lectin
189 receptors. We recently reported that the predominant ligand for Siglec-7 expressed on K562 cells
190 is the sialomucin CD43[17]. Further, we found that the commercially available MEM-59 antibody
191 binds to the same sialylated epitope on CD43 that is bound by Siglec-7[17]. We tested the ability of
192 AbLecs to compete with the MEM-59 antibody for binding to HER2+ K562 cells. We observed
193 that the T7 AbLec blocked binding of MEM-59 to a greater extent than trastuzumab or the non-
194 cognate T9 AbLec, suggesting that the T7 AbLec binds and blocks the same CD43 glycoform
195 bound by the endogenous Siglec-7 immunoreceptor (**Fig. 1l**). Taken together, this evidence
196 suggests that AbLecs selectively block engagement of the targeted lectin immunoreceptor by
197 competing for the same binding epitopes.

198

199 *AbLecs potentiate antibody-dependent phagocytosis and cytotoxicity of cancer cells*

200 Having demonstrated that AbLecs block binding of Siglec receptors to target cells, we
201 investigated whether AbLec treatment could enhance antibody-mediated cancer cell killing.
202 Therapeutic tumor-targeting antibodies create immune synapses between antigens on the cancer
203 cell surface and Fc receptors (FcRs) on immune cells. Engagement of FcRs activates the immune
204 cell to perform antibody effector functions including antibody-dependent cellular phagocytosis
205 (ADCP) and antibody-dependent cellular cytotoxicity (ADCC), which result in destruction of the
206 targeted cancer cell. However, Siglec ligands on the cancer cell surface recruit inhibitory Siglec
207 receptors to the immune synapse, dampening immune cell activation and restraining antibody

208 effector functions[12,16,43]. In contrast, we hypothesized that AbLecs would block Siglec engagement
209 at the immune synapse and enhance antibody effector functions (**Fig. 2a-b**).

210 We first tested our hypothesis using *in vitro* phagocytosis assays with primary human
211 macrophages (**Extended Data Fig. 3a, b**). At the time of use in our assays, macrophages
212 primarily expressed FcγRI and FcγRIIa (**Extended Data Fig. 3c, d**), as well as Siglecs-7 and -9
213 (**Extended Data Fig. 3e, f**). We co-cultured these macrophages with SK-BR-3 cells labeled with
214 a pH-sensitive dye that fluoresces red in acidic phagosomes (**Extended Data Fig. 3a**), enabling
215 quantification of phagocytosis via fluorescence. After 5 h of co-culture, fluorescence microscopy
216 images show that SK-BR-3 cells in co-cultures treated with the T7 AbLec are more readily
217 phagocytosed by macrophages compared to those treated with trastuzumab or Siglec-7-Fc decoy
218 receptor (**Fig. 2c**). We quantified the observed increase in phagocytosis using macrophages from
219 three unique donors and found that both T7 and T9 AbLecs significantly enhance phagocytosis
220 of tumor cells compared to trastuzumab or Siglec-Fc decoy receptors alone (**Fig. 2d; Extended**
221 **Data Fig. 4a, b**). We observed the same enhancement of phagocytosis of the HCC-1854 and
222 HER2+ K562 cell lines, which express varying levels of HER2 and/or Sig7/9L compared to SK-
223 BR-3 cells (**Extended Data Fig. 4c-j**).

224 We next asked whether AbLecs could potentiate cancer cell killing by additional subsets
225 of immune cells. We co-cultured primary human NK cells expressing FcγRIII and Siglec-7 with
226 SK-BR-3 tumor cells and analyzed cytotoxicity via flow cytometry (**Extended Data Fig. 5a-g**).
227 Across three donors, the T7 AbLec significantly enhanced NK cell cytotoxicity compared to
228 trastuzumab or Siglec-7-Fc decoy receptor (**Fig. 2e; Extended Data Fig. 5h, i**). We observed the
229 same effect in assays with the HER2+ K562 cell line (**Extended Data Fig. 5j, k**). We performed
230 similar assays with polymorphonuclear granulocytes (PMNs), which express FcγRIIa and
231 FcγRIII[26] as well as Siglecs-7 and -9 (**Extended Data Fig. 6a-d**). We found that T7 and T9 AbLecs
232 elicited increased tumor killing by PMNs compared to trastuzumab and AbLec isotype controls
233 (**Fig. 2f; Extended Data Fig. 6e-h**).

234 It was important to demonstrate that AbLec activity is at least partially antibody-dependent;
235 that is, mediated via antigen binding and FcR engagement. We observed that T7/9 AbLec-
236 mediated phagocytosis of target cells was dependent on expression of the HER2 antigen in
237 phagocytosis assays with WT (HER2-) and HER2+ K562 cells (**Fig. 2g**). To test FcR dependence,
238 we incubated macrophages with non-targeting antibodies of either rat IgG2a (rIgG2a) or human
239 IgG1 (hIgG1) isotype prior to co-culture with SK-BR-3 cells. The human IgG1 antibody competes
240 with both trastuzumab and T7 AbLec, which have hIgG1 Fc domains, to bind to macrophage
241 FcRs. In contrast, the rIgG2a isotype has very low affinity for human FcRs[44], and serves as a
242 negative control for FcR blockade. We observed lower levels of SK-BR-3 phagocytosis for both
243 trastuzumab and T7 AbLec when macrophages were pre-treated with hIgG1 isotype antibodies,
244 indicating that both antibody and AbLec activity is FcR-dependent (**Fig. 2h; Extended Data Fig.
245 7a**). We further found that an antibody blocking FcγRIII/CD16 significantly reduced AbLec-
246 mediated ADCC by NK cells, confirming that AbLec activity is FcR-dependent (**Extended Data
247 Fig. 7b**). Notably, FcR blockade appeared to reduce trastuzumab-mediated phagocytosis to a
248 greater extent than the T7 AbLec. Indeed, when we quantified the reduction in phagocytosis
249 observed upon FcR blockade across three unique donors we found that trastuzumab exhibited a
250 greater dependence on FcRs than the T7 AbLec (**Fig. 2i**). These data support our hypothesis that
251 AbLec mechanism of action is bifunctional, with contributions from activation of antibody effector
252 functions and glyco-immune checkpoint blockade. Overall, these results show that AbLecs elicit
253 enhanced antibody effector functions including ADCP and ADCC compared to their parent
254 monoclonal antibodies.
255
256 *AbLec efficacy is mediated via glyco-immune checkpoint blockade*
257 Critically, we tested whether AbLec-mediated enhancement of anti-tumor immune
258 responses was a result of blockade of Siglec-sialoglycan interactions. In these experiments, we
259 pre-incubated macrophages or NK cells with Siglec-7 or -9 blocking antibodies prior to co-culture

260 with SK-BR-3 cells (**Extended Data Fig. 7c, top**). If the targeted Siglec receptor was blocked,
261 AbLec-mediated ADCP (**Fig. 2j; Extended Data Fig. 7d**) and ADCC (**Fig. 2k; Extended Data**
262 **Fig. 7e**) were reduced to similar levels as those observed with trastuzumab treatment. However,
263 if Siglec receptors were not blocked, AbLec treatment enhanced ADCP (**Fig. 2j; Extended Data**
264 **Fig. 7d**) and ADCC (**Fig. 2k; Extended Data Fig. 7e**) compared to trastuzumab. We observed
265 the same evidence of Siglec dependence in ADCP and ADCC assays with HER2+ K562 cells
266 (**Extended Data Fig. 7f, g**). Pretreatment of target cells with sialidase to degrade Siglec ligands
267 also abolished AbLec-mediated enhancement of PMN ADCC over trastuzumab (**Extended Data**
268 **Fig. 6f, g**), further supporting the idea that AbLec activity is Siglec-dependent.

269 We further assessed the Siglec-dependence of AbLec activity in assays with murine bone
270 marrow-derived macrophages (BMDMs). We isolated BMDMs from WT mice and co-cultured
271 them with the syngeneic HER2+ B16D5 cell line, which expresses high levels of the HER2 antigen
272 and Sig9L, and intermediate levels of Sig7L (**Extended Data Fig. 8a-c**). We measured activation
273 of BMDMs via secretion of pro-inflammatory cytokines and chemokines upon treatment with
274 AbLecs and controls. We did not observe significant levels of BMDM activation upon treatment
275 with the T7 AbLec, perhaps due to the relatively low level of Sig7L expression on the HER2+
276 B16D5 cell line (**Extended Data Fig. 8a**). In contrast, T9 AbLec treatment significantly increased
277 BMDM activation (**Extended Data Fig. 8d-g**). We established similar models using BMDMs from
278 mice with engineered Siglec expression[20]. These included mice lacking Siglec-E, the murine
279 ortholog for human Siglec-7/9, and mice humanized for Sig7/9, in which SigE was knocked out
280 and human Sig7/9 receptors were knocked in (**Extended Data Fig. 8h**). In BMDMs from
281 humanized Sig7/9 mice, we observed an increase in BMDM activation in co-cultures treated with
282 T9 AbLec compared to those treated with trastuzumab. However, in SigE knockout mice, overall
283 activation was increased and activation upon T9 AbLec treatment was indistinguishable from
284 treatment with trastuzumab (**Extended Data Fig. 8i, j**). Taken together, these results suggest that

285 the increased levels of ADCP and ADCC observed with AbLec treatment are a direct result of

286 glycan blockade.

287

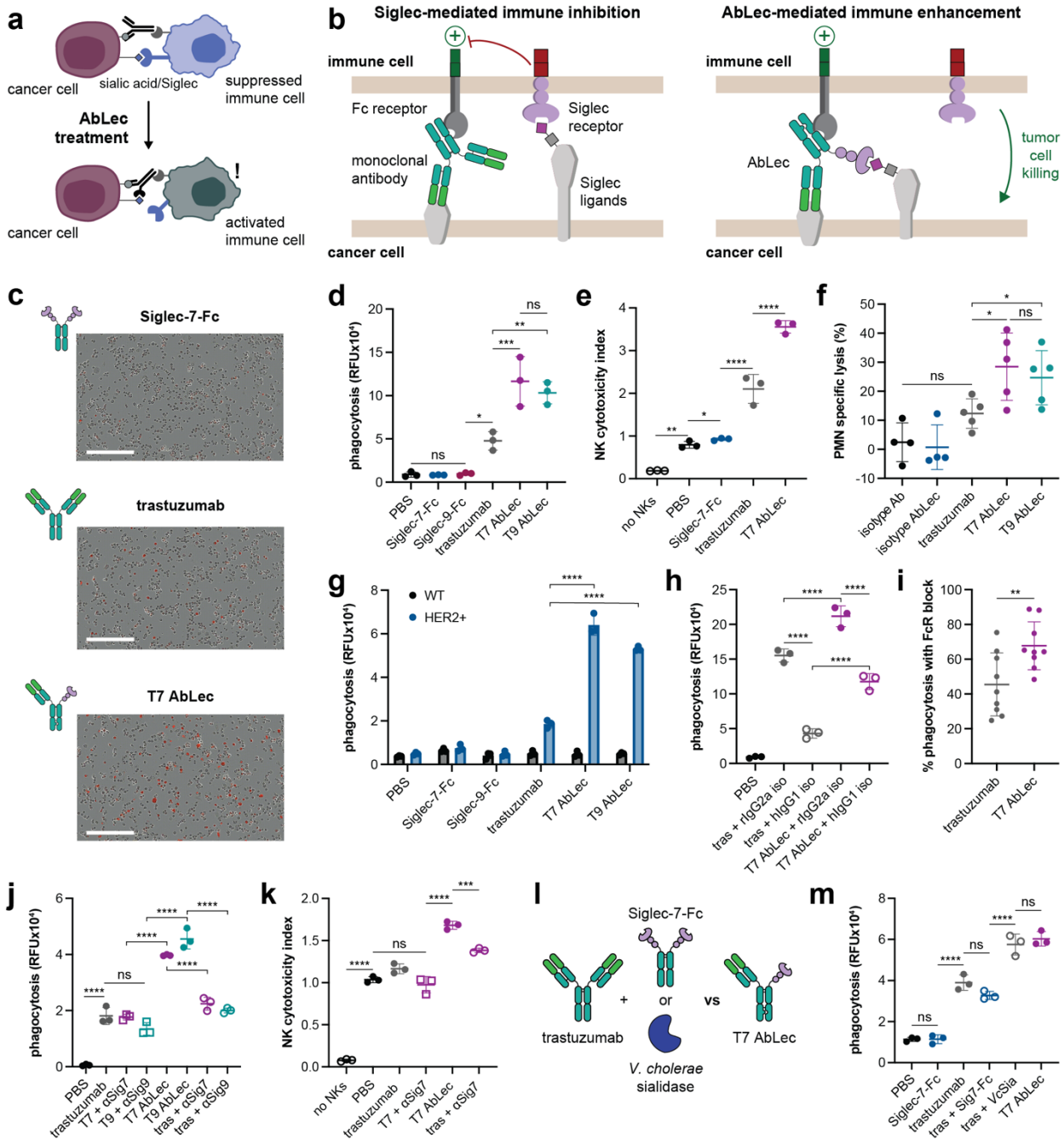

288

289 **Figure 2. AbLecs enhance antibody effector functions via glyco-immune checkpoint blockade.**

290 (**a**) Siglec engagement at immune synapses restrains anti-tumor immune responses. We hypothesize that
291 AbLecs will recruit FcR+ immune cells to tumors and simultaneously block Siglec engagement, relieving
292 inhibitory signaling and potentiating cancer cell killing.

293 (**b**) The chimeric AbLec architecture is designed to simultaneously elicit antibody effector functions via
294 FcR engagement and block binding of glyco-immune checkpoint receptors.

295 (**c**) Phase contrast and fluorescence microscopy images of primary human macrophage/SK-BR-3 cell co-
296 cultures treated with Siglec-7-Fc, trastuzumab, or T7 AbLec at t = 5 h. SK-BR-3 cells were stained with
297 the pHrodo red pH sensitive dye which fluoresces upon SK-BR-3 phagocytosis by macrophages. Images
298 are representative of n = 3 biological replicates, scale bar represents 400 μm.

299 (**d**) Phagocytosis of SK-BR-3 cells by primary human macrophages treated with T7/9 AbLecs,
300 trastuzumab, or Siglec-7/9-Fc. Data are mean ± s.d. of n = 3 biological replicates.

301 (**e**) Cytotoxicity of SK-BR-3 cells elicited by primary human NK cells treated with T7 AbLec, trastuzumab,
302 or Siglec-7-Fc. Data are mean ± s.d. of n = 3 biological replicates.

303 (**f**) Cytotoxicity of SK-BR-3 cells elicited by primary human granulocytes (PMNs) treated with T7/9
304 AbLecs, trastuzumab, or Siglec-7/9-Fc. Data are mean ± s.d. of biological replicates from n = 4-5 donors.

305 (**g**) Phagocytosis of HER2+ K562 cells compared to WT K562 cells, which are HER2-, (**Fig. 1h;**
306 **Extended Data Fig. 4c**) treated with T7/9 AbLecs, trastuzumab, or Siglec-7/9-Fc. Data are mean ± s.d. of
307 n = 3 biological replicates.

308 (**h**) Primary human macrophages were pre-treated with non-targeting antibodies to block human FcRs
309 (hIgG1 iso) or non-FcR binding controls (rIgG2a iso) prior to co-culture with SK-BR-3 cells and treatment
310 with trastuzumab (tras) or T7 AbLec. Data are mean ± s.d. of n = 3 biological replicates.

311 (**i**) Percent phagocytosis observed upon FcR blockade (+ hIgG1 iso RFU/+ rIgG2a iso RFU). Data are
312 mean ± s.d. of n = 3 biological replicates from each of n = 3 donors.

313 (**j**) Macrophage ADCP of SK-BR-3 cells induced by trastuzumab or T7/9 AbLecs in the presence or
314 absence of Siglec-7/9 blocking antibodies (αSig7 or αSig9, respectively). Data are mean ± s.d. of n = 3
315 biological replicates.

316 (**k**) NK cell ADCC of SK-BR-3 cells induced by trastuzumab or T7 AbLec in the presence or absence of a
317 Siglec-7 antagonist antibody (αSig7). Data are mean ± s.d. of n = 3 biological replicates.

318 (**l**) We compared combination of trastuzumab with Siglec-7-Fc or *V. cholerae* sialidase (*Vc*Sia) to T7
319 AbLec treatment in their ability to activate macrophage ADCP.

320 (**m**) Macrophage ADCP of HER2+ K562 cells treated with Siglec-7-Fc, trastuzumab, T7 AbLec, or
321 combinations of trastuzumab with Siglec-7-Fc or *V. cholerae* sialidase (*Vc*Sia). Data are mean ± s.d. of n
322 = 3 biological replicates.

323

324 *The chimeric AbLec architecture enables potent glyco-immune checkpoint antagonism*

325 Combination of monospecific therapies results in enhanced therapeutic efficacy, and is
326 now thought to be required for durable responses in most cancer patients[45]. We hoped the
327 bispecific AbLec architecture would elicit tumor-targeted antibody effector functions and glyco-
328 immune checkpoint blockade at least as effectively as combination therapy. Thus, we sought to
329 benchmark efficacy of AbLecs compared to combinations of trastuzumab with existing Siglec

330 blockade approaches. First, we compared AbLec treatment to combinations of trastuzumab with
331 Siglec blocking antibodies[20] (**Extended Data Fig. 7c, bottom**). Surprisingly, AbLecs elicited
332 enhanced ADCP (**Fig. 2j**) and ADCC (**Fig. 2k**) of SK-BR-3 cells compared to the combination of
333 trastuzumab with Siglec-7 or -9 antagonist antibodies[20]. We observed the same trends in ADCP
334 and ADCC assays with HER2+ K562 cells (**Extended Data Fig. 7f, g**). These data suggest that
335 blockade of Siglec engagement locally, at the immune synapse, could be more effective than
336 systemic Siglec antagonism.

337 We further compared AbLec efficacy to combination of trastuzumab with *Vibrio cholerae*
338 sialidase as a model of enzymatic sialoglycan degradation, an approach to target the Siglec/sialic
339 acid axis that is currently being investigated in clinical trials[34] (**Fig. 2l**). The *Vibrio cholerae*
340 sialidase cleaves all linkages (α2,3; α2,6; and α2,8) of terminal sialic acid, blocking Siglec
341 engagement via ligand degradation[12,16]. There was no significant difference in ADCP elicited by
342 T7 AbLec treatment compared to the combination of trastuzumab with *V. cholerae* sialidase (**Fig.
343 2l; Extended Data Fig. 9a, b**). Combination of T7 and T9 AbLecs did not further enhance ADCP
344 compared to T7 or T9 treatment alone (**Extended Data Fig. 9c, d**). Similarly, activation of murine
345 BMDMs treated with T9 AbLec was indistinguishable from combination treatment with
346 trastuzumab with *V. cholerae* sialidase (**Extended Data Fig. 8d-g**). These data indicate that
347 AbLec-mediated Siglec blockade is as effective as sialic acid degradation in its ability to potentiate
348 antibody effector functions.

349 We asked whether the chimeric AbLec architecture was required to potentiate tumor
350 killing. To do this, we compared phagocytosis in macrophage/HER2+ K562 cell cultures treated
351 with T7 AbLec or the combination of trastuzumab with the Siglec-7-Fc decoy receptor (**Fig. 2l**).
352 We found that combination of trastuzumab with Siglec-7-Fc did not enhance killing of HER2+
353 K562 cells compared to trastuzumab alone, as expected given the low binding affinity of the decoy
354 receptor (**Fig. 2m; Extended Data Fig. 9a, b**). However, as before, treatment with T7 AbLec
355 elicited enhanced tumor phagocytosis (**Fig. 2m; Extended Data Fig. 9a, b**). From these results,

356 we conclude that the chimeric AbLec architecture is required to recruit lectin decoy receptor
357 domains to tumor cell surfaces at therapeutically relevant concentrations and potentiate tumor
358 killing.

359 Overall, our findings support the paradigm that the chimeric AbLec architecture results in
360 a gain-of-function: the ability to block inhibitory signaling through glyco-immune checkpoints.
361 AbLecs are more effective glyco-immune checkpoint antagonists than Siglec-blocking antibodies,
362 and as effective as enzymatic sialic acid degradation, both of which are therapeutic strategies
363 being investigated in clinical trials[33,34].

364

365 *The AbLec platform is extensible to multiple cancers and mechanisms of action*

366 Due to their modular chimeric architecture, AbLecs can be readily developed to target
367 diverse cancers and glyco-immune checkpoints. To demonstrate this modularity, we constructed
368 tumor-targeting AbLecs with components derived from rituximab x Siglec-7 (R7) and cetuximab x
369 Siglec-7 (C7), designed to block Sig7L on CD20+ and EGFR+ cancer cells, respectively (**Fig. 3a,**
370 **b**). In addition, we generated a trastuzumab x Siglec-10 AbLec that simultaneously targets HER2+
371 tumors while blocking engagement of the Siglec-10 receptor, which was recently shown to
372 mediate immune evasion in breast and ovarian cancers[15] (**Fig. 3c**).

373 We further developed dual checkpoint blockade AbLecs designed to block engagement
374 of both protein and glycan-based checkpoint receptors. We designed an AbLec for dual blockade
375 of the "don't eat me" signal CD47 and Siglec-7 ligands on tumor cells by combining the clinical-
376 stage αCD47 antibody magrolimab[46] with a Siglec-7 decoy receptor domain (**Fig. 3d**). We
377 generated nivolumab x galectin-9 and pembrolizumab x galectin-9 AbLecs designed to
378 simultaneously block the PD-1/PD-L1 and TIM-3/galectin-9 T cell checkpoints (**Fig. 3e, f**).
379 Nivolumab and pembrolizumab are PD-1 blocking antibodies approved to treat diverse cancers[47–
380 55]. Notably, the galectin-9 lectin is a ligand for the TIM-3 checkpoint receptor, and binding of
381 galectin-9 to TIM-3 contributes to CD8+ T cell exhaustion[38,56]. Both galectin-9 and TIM-3

382 antagonist antibodies are cancer immunotherapy approaches being investigated in clinical
383 trials[32,57–59]. Finally, we used the binding domain from the FDA-approved αPD-L1 antibody
384 avelumab[60–62] to engineer an avelumab x Siglec-7 AbLec for dual blockade of PD-L1 and Sig7L
385 expressed on tumor or antigen presenting cells (**Fig. 3g**).

386 Functional characterization of R7 and C7 AbLecs demonstrated the utility of the AbLec
387 platform for combination tumor targeting and glyco-immune checkpoint blockade in diverse tumor
388 types. Across n = 3 unique donors, R7 and C7 AbLecs significantly enhanced phagocytosis of
389 CD20+ Ramos cells or EGFR+ K562 cells compared to the parent antibody or Siglec-7-Fc alone
390 (**Fig. 3h, i; Extended Data Fig. 9e-j**). Importantly, and consistent with our findings with T7/9
391 AbLecs, R7 and C7 AbLecs selectively target antigen expressing cells and spare antigen negative
392 cells (**Fig. 3j-o**). Thus, AbLecs can be readily redesigned to target a variety of cancer antigens.

393 Low or heterogeneous expression of tumor-associated antigens on cancer cell surfaces
394 has been associated with resistance to immunotherapies including monoclonal antibodies[63,64],
395 immune checkpoint blockade[65], and CAR-T cells[66,67]. We hypothesized that the enhanced effector
396 functions elicited by AbLecs might be able to overcome weak FcR signaling potentiated by tumors
397 with low antigen density. We created K562 lines expressing high and low levels of the CD20
398 antigen, while the expression of Sig7L was constant (**Fig. 3j-l**). In assays with primary human
399 macrophages, we found that R7 AbLec treatment enhanced ADCP of tumor cells expressing very
400 low levels of the targeted CD20 antigen compared to the parent monoclonal antibody, rituximab
401 (**Fig. 3j-l, n**). Our results show that the improved efficacy of AbLecs compared to the parent
402 monoclonal antibody is maintained in cancers with low antigen expression, a current area of
403 unmet medical need.
404

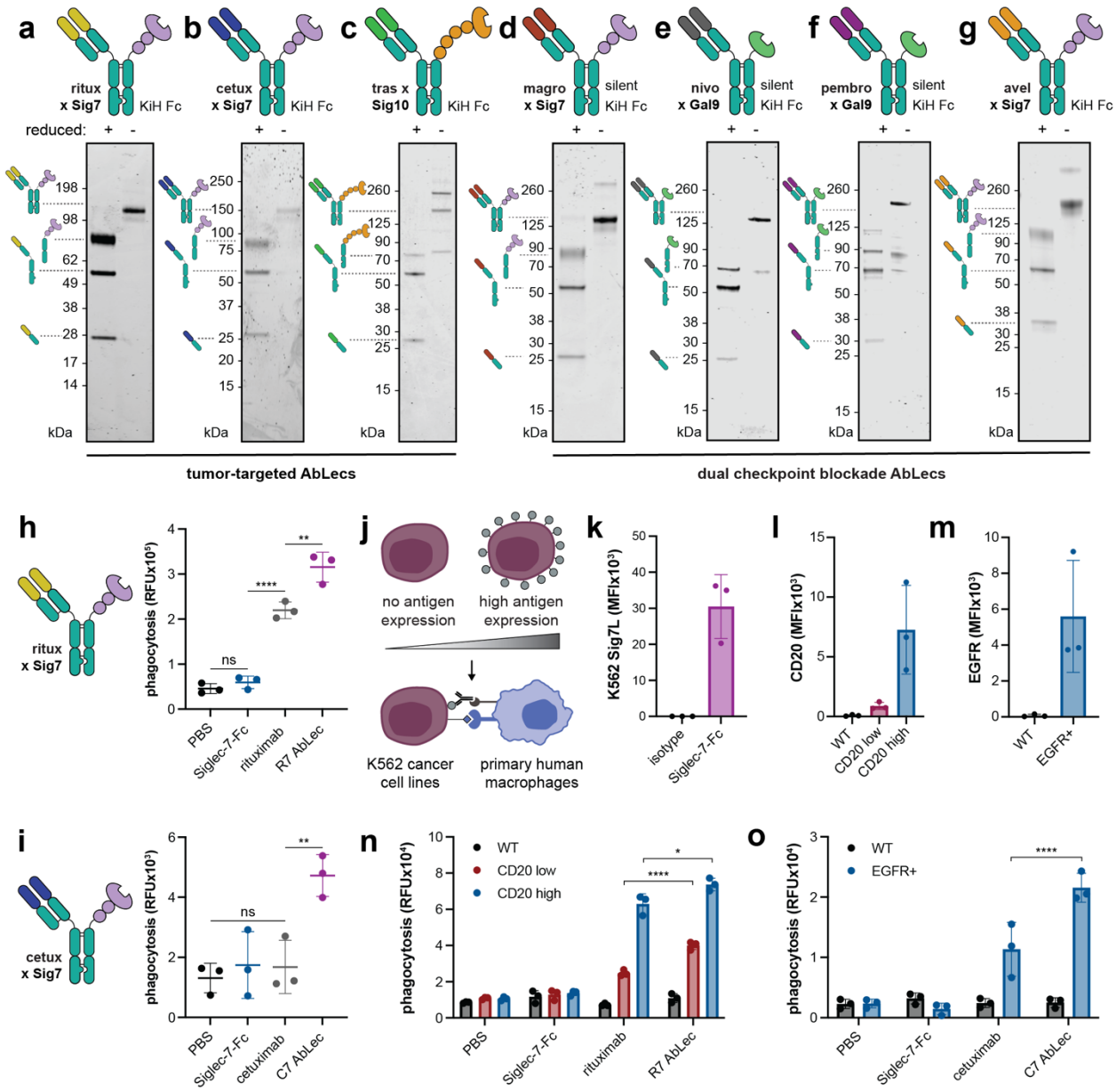

Figure 3. The AbLec platform is extensible to multiple cancers and mechanisms of action.

(**a-g**) Reducing (+) and non-reducing (-) SDS-PAGE analysis of purified (**a**) rituximab (αCD20) x Siglec-7 (R7) AbLec, (**b**) cetuximab (αEGFR) x Siglec-7 (C7) AbLec, (**c**) trastuzumab (αHER2) x Siglec-10 (T10) AbLec, (**d**) magrolimab (αCD47) x Siglec-7 (M7) AbLec, (**e**) nivolumab (αPD-1) x Galectin-9 (NG9) AbLec, (**f**) pembrolizumab (αPD-1) x Galectin-9 (PG9) AbLec, and (**g**) avelumab (αPD-L1) x Siglec-7 (A7) AbLec. Gels are representative of n = 3 replicates.

(**h**) ADCP of Ramos cells by primary human macrophages in co-cultures treated with R7 AbLec, rituximab, or Siglec-7-Fc. Data are mean ± s.d. of n = 3 biological replicates.

(**i**) ADCP of EGFR+ K562 cells by primary human macrophages in co-cultures treated with C7 AbLec, cetuximab, or Siglec-7-Fc. Data are mean ± s.d. of n = 3 biological replicates.

(**j**) We engineered K562 cell lines expressing high and low levels of tumor-associated antigens (CD20, EGFR). WT K562s were antigen negative. These cell lines were used to interrogate AbLec efficacy in tumors with low antigen density.

419 (**k**) Sig7L expression measured via Siglec-7-Fc staining of K562 cells compared to hIgG1 isotype control.
420 Data are mean ± s.d. of n = 3 biological replicates.

421 (**l**) CD20 expression on WT, CD20 low, and CD20 high K562 cells measured via rituximab staining
422 compared to hIgG1 isotype antibody by flow cytometry. Data are mean ± s.d. of n = 3 biological
423 replicates.

424 (**m**) EGFR expression on WT and EGFR+ K562 cells measured via cetuximab staining compared to
425 hIgG1 isotype antibody by flow cytometry. Data are mean ± s.d. of n = 3 biological replicates.

426 (**n**) Macrophage ADCP of WT, CD20 low, and CD20 high K562 cells treated with R7 AbLec, rituximab, or
427 Siglec-7-Fc. Data are mean ± s.d. of n = 3 biological replicates.

428 (**o**) Macrophage ADCP of WT and EGFR+ K562 cells treated with C7 AbLec, cetuximab, or Siglec-7-Fc.
429 Data are mean ± s.d. of n = 3 biological replicates.

430

431 *AbLecs synergize with blockade of established immune checkpoints*

432 Siglecs and sialic acids are upregulated in patients that do not respond to PD-1 blockade[27],
433 suggesting that glyco-immune checkpoints are an orthogonal mechanism of immune evasion in
434 the tumor microenvironment. If this is true, we would expect AbLecs to synergize with existing
435 checkpoint blockade modalities. We tested this hypothesis by investigating whether trastuzumab
436 hybrid AbLecs synergize with blockade of CD47, in light of recent results showing that CD47
437 blockade synergizes with trastuzumab[68]. If glyco-immune checkpoints are a distinct axis of
438 immune suppression, we would expect the combination of trastuzumab hybrid AbLecs with CD47
439 blockade to further enhance ADCP of HER2+ cancer cells (**Fig. 4a**). Indeed, combination of a
440 CD47 antagonist antibody and T7 AbLec elicited enhanced tumor killing compared to T7 AbLec
441 treatment alone in 2 of 3 donors tested (**Fig. 4b; Extended Data Fig. 10a-c**). Across all 3 donors,
442 combination of αCD47 and T7 AbLec outperformed the combination of αCD47 and trastuzumab
443 (**Extended Data Fig. 10a-c**). Combination of αCD47 and T7 AbLec also enhanced PMN
444 cytotoxicity over αCD47 and trastuzumab (**Extended Data Fig. 6h**).

445 In light of this finding, we designed dual checkpoint blockade AbLecs to enable blockade
446 of protein- and glycan-based checkpoints with a single chimeric molecule. We first characterized
447 AbLecs targeting the PD-1/PD-L1 and TIM-3/galectin-9 checkpoints on T cells, which combined
448 the nivolumab or pembrolizumab αPD-1 antibody binding domains with the glycan-binding domain
449 from galectin-9 (NG9 and PG9 AbLecs, respectively; **Fig. 4c**). We found that both AbLecs bound

450 to activated human T cells at nanomolar concentrations (**Fig. 4d-f; Extended Data Fig. 10d**).
451 Further, NG9 and PG9 AbLecs exhibited distinct binding profiles compared to parent monoclonal
452 antibody and galectin-9-Fc controls (**Fig. 4e, f**), indicating contributions from both αPD-1 and
453 galectin-9 domains to overall AbLec binding.

454 Finally, we asked whether dual checkpoint blockade AbLecs were functional (**Fig. 4g**).
455 The A7 AbLec combines the Fab domain from the αPD-L1 antibody avelumab with the glycan-
456 binding domain from Siglec-7 for dual blockade of the PD-1/PD-L1 and Siglec-7/sialic acid
457 immunological axes. A7 AbLec enhanced phagocytosis of MDA-MB-231 cells expressing PD-L1
458 and Sig7L compared to the avelumab antibody alone (**Fig 4h; Extended Data Fig. 10e-g**). Taken
459 together, AbLecs target an orthogonal immunosuppressive pathway in cancer and can be used
460 alone or in combination with existing clinical-stage immunotherapies to drive enhanced antitumor
461 immune responses.
462

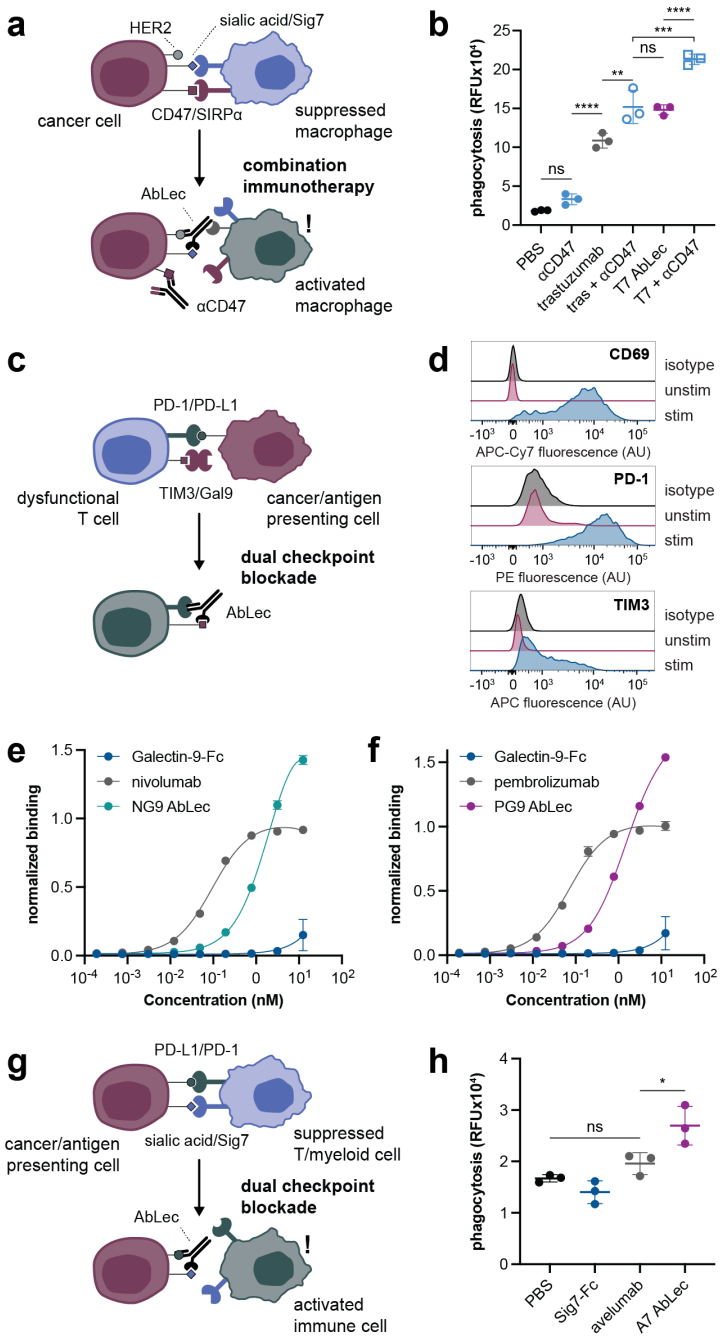

Figure 4. AbLecs target a distinct axis of immune regulation and can be used to simultaneously block protein- and glycan-based immune checkpoints.

(**a**) We tested the ability of T7 AbLec treatment to synergize with CD47 blockade in ADCP assays with primary human macrophages.

(**b**) ADCP of SK-BR-3 cells by primary human macrophages in co-cultures treated with trastuzumab or T7 AbLec alone and in combination with a CD47 antagonist antibody. Data are mean ± s.d. of n = 3 biological replicates.

(**c**) We developed dual checkpoint blockade AbLecs to simultaneously block the PD-1/PD-L1 and TIM-3/galectin-9 T cell checkpoints.

473 (**d**) Following 3 days of stimulation with αCD3/αCD28 antibodies, primary human CD3+ T cells
474 upregulated CD69, PD-1, and TIM-3 by flow cytometry compared to unstimulated T cell and isotype
475 controls.

476 (**e-f**) NG9 (**e**) and PG9 (**f**) AbLecs bind to activated human CD3+ T cells at nanomolar concentrations.
477 Data are mean ± s.d. of n = 3 biological replicates.

478 (**g**) We developed dual checkpoint blockade AbLecs to simultaneously block the PD-1/PD-L1 and Siglec-
479 7 checkpoints that negatively regulate activation of both T cells and myeloid cells.

480 (**h**) Phagocytosis of MDA-MB-231 cells by primary human macrophages in co-cultures treated with A7
481 AbLec, avelumab (αPD-L1), or Siglec-7-Fc. Data are mean ± s.d. of n = 3 biological replicates.

482

483 ## Discussion

484 In this work, we establish AbLecs as a new class of antibody chimeras targeting glyco-
485 immune checkpoints for cancer immunotherapy. AbLecs combine antibodies targeting antigens
486 of interest (e.g., tumor-associated antigens, immune checkpoint receptors or ligands) with glycan-
487 binding domains from immunomodulatory lectin receptors. We show that AbLecs bind to cell
488 surfaces at therapeutically relevant concentrations and selectively block binding of the targeted
489 lectin receptor. Tumor-targeted AbLecs potentiated antibody effector functions including
490 phagocytosis and cytotoxicity of cancer cells, including those with low expression of the targeted
491 antigen. Synergy with blockade of established checkpoints demonstrated the potential for AbLecs
492 to expand the subset of patients that benefit from cancer immunotherapy. Overall, AbLecs offer
493 a modular molecular architecture for glycan blockade as a unique immunotherapeutic mechanism
494 of action.

495 Unexpectedly, we found that T7 and T9 AbLecs were more effective Siglec antagonists
496 than Siglec-blocking antibodies and as effective as sialoside degradation. This result suggests
497 that proximity of the tumor-targeting and Siglec blockade elements may be important. This idea
498 is consistent with a recent study demonstrating that Siglec recruitment to FcRs can fully inhibit
499 FcR activation[43]. Similarly, emerging evidence indicates that recruitment of cell-surface
500 phosphatases to immunoreceptors inhibits their activation[69], while phosphatase exclusion
501 potentiates signaling[70]. In light of these findings, we propose that the ability of tumor-targeted
502 AbLecs to enhance immune cell activation is mediated via exclusion of inhibitory lectin receptors

503 from the immunological synapse. Our data suggests that targeted lectin blockade mediated by
504 AbLecs is at least as effective as systemic glyco-immune checkpoint blockade with the potential
505 for reduced toxicity.

506 Tumors dramatically remodel their cell surface glycosylation. It is now clear that a key role
507 for these remodeled glycans is to facilitate immune evasion and tumor progression by engaging
508 multiple broad classes of lectin immunoreceptors[10–27,37,38,71–79]. Our chimeric AbLec molecules
509 result in a gain-of-function: the ability to block glyco-immune checkpoints that represent an
510 important mechanism of immune suppression and therapeutic resistance in cancer. The AbLec
511 approach is extensible to multiple cancers and mechanisms of action, with the potential to expand
512 the efficacy of cancer immunotherapy.

513

514 **Methods**

515 *Cell lines*

516 All cell lines were purchased from the American Type Culture Collection (ATCC) unless otherwise
517 noted. SK-BR-3, HCC-1954, K562, and Ramos cells were cultured in RPMI + 10% fetal bovine
518 serum (FBS) without antibiotic selection. HER2+ B16D5 cells were a gift from the Weiner
519 laboratory (Lombardi Cancer Center) and were cultured in DMEM with 10% FBS, 1% glutamine,
520 1% sodium pyruvate and 1% amino acids and without antibiotic selection. MDA-MB-231 cells
521 were cultured in DMEM with 10% FBS, 1% glutamine, 1% sodium pyruvate and 1% amino acids
522 and without antibiotic selection. Expi293F cells were a gift from the Kim lab at Stanford and were
523 cultured according to the manufacturer protocol (Thermo Fisher Scientific) protocol. K562s were
524 transfected according to manufacturer's protocol with EGFR using pre-packaged lentiviral
525 particles (G&P Biosciences) and selected for EGFR expression by culture in 1 μg/mL puromycin
526 (InVivoGen). K562s were transfected according to manufacturer's protocol with CD20 using pre-
527 packaged lentiviral particles (G&P Biosciences) and sorted for high and low CD20 expressing

528 cells using rituximab and a BV421-labeled anti-human secondary (Jackson ImmunoResearch).
529 Lentiviral vector encoding *HER2/neu* was a gift from Mien-Chie Hung (Addgene plasmid #16257).
530 Stable $HER2^+$ cell lines were generated as previously described[80] and HER2 expression was
531 verified by flow cytometry. Cell lines were not independently authenticated beyond the identity
532 provided by the ATCC. Cell lines were cultivated in a humidified incubator at 5% CO_2 and 37 ºC
533 and tested negative for mycoplasma quarterly using a PCR-based assay.
534
535 *Plasmids and protein sequences*
536 All antibody and AbLec plasmids were generated by Twist Bioscience and inserted into the pTwist
537 CMV BetaGlobin vector using the XhoI and NheI cut sites, unless otherwise specified below. DNA
538 and amino acid sequences are listed in **Supplemental Table 1**. Trastuzumab was expressed
539 from a pCDNA3.1 vector described in our previous work[16]. The rituximab and cetuximab antibody
540 variable sequences were generated by IDT and cloned into the variable regions of the VRC01
541 antibody plasmid vector (a generous gift from the Kim lab at Stanford) by using the In-Fusion
542 cloning kit (Takara) according to the manufacturer's protocol. The EndoFree Plasmid Maxi Kit
543 (Qiagen) was used to prepare DNA for transfection.
544
545 *Protein expression and purification*
546 Antibodies and AbLecs were expressed via transient transfection in Expi293F cells (Thermo
547 Fisher Scientific) according to the manufacturer protocol. For antibodies, a 1:1 heavy to light chain
548 plasmid ratio by weight was used. The trastuzumab antibody heavy chain and light chain were
549 co-expressed from a single plasmid. For AbLecs, a 2:1:1 ratio of lectin:heavy chain:light chain
550 was used. After seven days of expression, proteins were collected from the supernatant by
551 pelleting cells at 500 *x g* for 5 min, followed by clarification with a spin at 4000 *x g* for 40 min, and
552 0.2 µm filtration. Antibodies were purified by manual gravity column (BioRad) using protein A
553 agarose (Fisher Scientific). Briefly, the clarified supernatant was flowed over the column twice,

554 bound protein was sialidase treated on the resin with 0.25-0.5 column volumes of 100 nM *V.*
555 *cholerae* sialidase in PBS for 0.5-2 h rt, washed with 20 column volumes of PBS, and eluted twice
556 with 5 mL 100 mM glycine buffer pH 2.8 into tubes pre-equilibrated with 150 µL of 1 M Tris pH 8.
557 AbLecs were purified by manual gravity column using nickel-NTA agarose resin (Qiagen). Briefly,
558 AbLec supernatant was incubated with PBS-equilibrated resin for ~1 hour at 4 °C. Resin and
559 supernatant was then loaded onto a chromatography column, bound protein was sialidase treated
560 on the resin with 0.25-0.5 column volumes of 100 nM *V. cholerae* sialidase in PBS for 0.5-2 h rt,
561 washed with 20 column volumes PBS + 20 mM imidazole, and eluted twice with 5 column volumes
562 PBS + 250 mM imidazole. Antibodies and AbLecs were buffer exchanged into PBS using PD-10
563 desalting columns (GE). Purified avelumab monoclonal antibody was purchased from Selleck
564 Chemicals.
565
566 *AbLec gel characterization*
567 For SDS-PAGE gels, 2 µg of protein with SDS loading dye (non-reducing conditions), or SDS dye
568 + 1 M betamercaptoethanol, heated at 95 °C for 5 min (reducing conditions), were loaded onto a
569 Criterion™ XT 4-12% Bis-Tris Protein Gel, 18 well, (Bio-Rad) and run with XT-MES buffer at 180
570 V for 40 min. Total protein content was visualized using Aquastain (Bulldog Bio) with staining for
571 10 minutes followed by a 10 minute destain in water. For AbLec Western blots, 0.2 µg of protein
572 was loaded onto an SDS-PAGE gel and run as described above, transferred to a nitrocellulose
573 membrane using the Trans-Blot® Turbo™ RTA Midi Nitrocellulose Transfer Kit (Bio-Rad) at 25V,
574 for 14 min. The membrane was blocked in Intercept® PBS blocking buffer (LI-COR) for 0.5-1 h rt,
575 then stained with anti-HA Tag Polyclonal Antibody (clone SG77, Thermo Fisher Scientific; 1:500)
576 and anti-6xHis antibody (clone J099B12, BioLegend; 1:2000) for 1 hour in Intercept® PBS
577 blocking buffer with shaking at rt. The membrane was washed 3x in PBST (PBS + 0.1% Tween),
578 followed by staining with secondary antibodies IRDye® 800CW Goat anti-Mouse and IRDye®
579 680RD Goat anti-Rabbit (LI-COR; 1:15,000) in PBST for 0.5-1 h with shaking at room temp,

580 followed by 3x washes in PBST before imaging. All gels and blots were imaged on an Odyssey®
581 CLx Imaging System (LI-COR).
582
583 *AbLec mass spectrometry characterization*
584 Four micrograms of each AbLec were digested with trypsin for proteomic analysis. Samples were
585 incubated for 15 minutes at 55 °C with 5 mM dithiothreitol, followed by a 30 minute incubation at
586 room temperature in the dark with 15 mM iodoacetamide. Trypsin (Promega) was added at a 1:20
587 w:w ratio and digestions proceeded at room temperature overnight. The following morning,
588 samples were desalted by quenching the digestion with formic acid to a final pH of ~2, followed
589 by desalting over a polystyrene-divinylbenzene solid phase extraction (PS-DVB SPE) cartridge
590 (Phenomenex). Samples were dried with vacuum centrifugation following desalting and were
591 resuspended in 0.2% formic acid in water at 0.5 µg per µL.
592
593 Approximately 1 µg of peptide was injected per analysis, wherein peptides were separated over
594 a 25 cm EasySpray reversed phase LC column (75 µm inner diameter packed with 2 µm, 100 Å,
595 PepMap C18 particles, Thermo Fisher Scientific). The mobile phases (A: water with 0.2% formic
596 acid and B: acetonitrile with 0.2% formic acid) were driven and controlled by a Dionex Ultimate
597 3000 RPLC nano system (Thermo Fisher Scientific). Gradient elution was performed at 300
598 nL/min. Mobile phase B was held at 0% over 6 min, followed by an increase to 5% at 7 minutes,
599 25% at 66 min, a ramp to 90% B at 70 min, and a wash at 90% B for 5 min. Flow was then ramped
600 back to 0% B at 75.1 minutes, and the column was re-equilibrated at 0% B for 15 min, for a total
601 analysis time of 90 minutes. Eluted peptides were analyzed on an Orbitrap Fusion Tribrid MS
602 system (Thermo Fisher Scientific). Precursors were ionized using an EASY-Spray ionization
603 source (Thermo Fisher Scientific) source held at +2.2 kV compared to ground, and the column
604 was held at 40 °C. The inlet capillary temperature was held at 275 °C. Survey scans of peptide
605 precursors were collected in the Orbitrap from 350-1350 m/z with an AGC target of 1,000,000, a

606 maximum injection time of 50 ms, and a resolution of 60,000 at 200 m/z. Monoisotopic precursor
607 selection was enabled for peptide isotopic distributions, precursors of z = 2-5 were selected for
608 data-dependent MS/MS scans for 2 seconds of cycle time, and dynamic exclusion was set to 30
609 seconds with a ±10 ppm window set around the precursor monoisotope. An isolation window of
610 1 m/z was used to select precursor ions with the quadrupole. MS/MS scans were collected using
611 HCD at 30 normalized collision energy (nce) with an AGC target of 100,000 and a maximum
612 injection time of 54 ms. Mass analysis was performed in the Orbitrap a resolution of 30,000 at
613 200 m/z and scan range set to auto calculation.
614
615 Raw data were processed using Byonic[81] in MaxQuant version 3.11.3. Oxidation of methionine
616 (+15.994915) was set as a common[82] variable modification, protein N-terminal acetylation
617 (+42.010565) and asparagine deamination (+0.984016) were specified as rare variable
618 modifications, and carbamidomethylation of cysteine (+57.021464) was set as a fixed
619 modification. Up to three common and two rare modifications were permitted. A precursor ion
620 search tolerance of 10 ppm and a product ion mass tolerance of 20 ppm were used for searches,
621 and three missed cleavages were allowed for full trypsin specificity. Peptide spectral matches
622 (PSMs) were made against custom FASTA sequence files that contained appropriate
623 combinations of Siglec-7 and -9 holes, and trastuzumab knobs and light chains. Peptides were
624 filtered to a 1% false discovery rate (FDR) and a 1% protein FDR was applied according to the
625 target-decoy method. All peptide identifications were manually inspected, and sequences
626 coverages were calculated only from validated peptide identifications. Sequence coverage
627 percentages are derived from the proportion of amino acids explained by peptide identifications
628 relative to the total number of amino acids.
629
630 *Lectin flow cytometry*

631 Cells were pelleted by centrifugation, washed once with phosphate-buffered saline (PBS), and
632 resuspended in FACS buffer (PBS with 0.5% bovine serum albumin). Siglec-Fc or human IgG1
633 isotype Fc (R&D Systems) precomplexes with Alexa Fluor 647 (AF647)-labeled donkey anti-
634 human IgG antibody (Jackson ImmunoResearch) were prepared at equimolar concentrations (7.5
635 nM) in FACS buffer. Biotin-labeled MALII lectin (Vector Labs, 10 μg/mL) was precomplexed with
636 AF647-Streptavidin (Thermo Fisher Scientific, 1 μg/mL) in FACS buffer. Staining was performed
637 for 30 min on ice at 1×10^6 cells/mL. Cells were subsequently washed twice with ice-cold FACS
638 buffer, resuspended in FACS buffer containing 100 nM SytoxGreen or 1 μM SytoxBlue (Thermo
639 Fisher Scientific), and analyzed by flow cytometry (BD LSR II).
640
641 *Antibody flow cytometry*
642 Cells were pelleted by centrifugation, washed once with phosphate-buffered saline (PBS), and
643 resuspended in FACS buffer, as above. To quantify HER2, CD20, or EGFR expression, cells
644 were stained with 7.5 nM antibody (trastuzumab, rituximab, or cetuximab, respectively) or a
645 human IgG1 isotype control in FACS buffer for 30 min on ice at 1×10^6 cells/mL. Cells were
646 subsequently washed twice with ice-cold FACS buffer, resuspended in FACS buffer with 7.5 nM
647 AF647-labeled donkey anti-human IgG secondary antibody (Jackson ImmunoResearch) and
648 stained for 30 min on ice. Following incubation with the secondary antibody, cells were washed
649 twice with ice-cold FACS buffer, resuspended in FACS buffer containing 100 nM SytoxGreen or
650 1 μM SytoxBlue (Thermo Fisher Scientific), and analyzed via flow cytometry (BD LSR II). For all
651 other flow experiments, cells were stained with 10 μg/mL dye-labeled antibodies or the
652 appropriate isotype controls in FACS buffer for 30 min at 4 ºC. All antibody clones used are listed
653 in **Supplemental Table 2**. Following incubation, cells were washed twice with ice-cold FACS
654 buffer, resuspended in FACS buffer containing 100 nM SytoxGreen or 1 μM SytoxBlue (Thermo
655 Fisher Scientific), and analyzed via flow cytometry (BD LSR II).
656

657 *Quantifying AbLec binding and K_D*

658 HER2+ K562 and SK-BR-3 cells were isolated from the cell culture supernatant or via dissociation
659 with TrypLE (Gibco), respectively, washed with 1xPBS, and resuspended in blocking buffer.
660 60,000 cells were then distributed into wells of a 96-well V-bottom plate (Corning). Various
661 concentrations of trastuzumab, nivolumab, pembrolizumab, Siglec-Fcs (R&D Systems), Galectin-
662 9-Fc (Sino Biological), or AbLecs were added to the cells in equal volumes and incubated with
663 cells for 1 h at 4 °C with periodic pipet mixing. Cells were washed three times in FACS buffer
664 (PBS + 0.5% bovine serum albumin), pelleting by centrifugation at 300 xg for 5 min at 4 °C
665 between washes. Cells were resuspended in 4 μg/mL AF647-labeled donkey anti-human
666 secondary antibody (Jackson ImmunoResearch) in FACS buffer for 30 min at 4 °C. Cells were
667 further washed twice and resuspended in FACS buffer, and fluorescence was analyzed by flow
668 cytometry (BD LSR II). Gating was performed using FlowJo v.10.0 software (Tree Star) to
669 eliminate debris and isolate single cells. Mean fluorescence intensity (MFI) of the cell populations
670 were normalized to the MFI of cells stained with 50 nM trastuzumab from each experimental
671 replicate. MFI values were fit to a one-site total binding curve using GraphPad Prism 9.0, which
672 calculated the K_D values as the antibody concentration needed to achieve a half-maximum
673 binding.

674

675 *Computational modeling of AbLec binding and apparent ligand concentrations*

676 The *MVsim* multivalent simulation application (version 1.1 with MATLAB 2021a) was used to
677 model trastuzumab, T7 AbLec, and T7A AbLec binding to HER2+ K562 cells, as previously
678 reported[42]. *MVsim* models the effects of molecular valency, topology, affinity, and kinetics on the
679 binding dynamics of multivalent and multispecific macromolecular receptor-ligand systems. Here,
680 the *MVsim* application was used to create a modeling routine that simulated, via the microstate
681 binding model[42], the interaction of antibodies and antibody-like chimeras to surfaces populated
682 with specific targeted ligands/antigens. The designed sequences and structures of the

683 biomolecules were used to parameterize the model with the binding valencies. Here, the
684 trastuzumab, T7A AbLec, and Siglec-7-Fc reference biomolecules, as well as the T7 AbLec, were
685 modeled as topologically related, Fc domain-driven, immunoglobulin dimers, each with a valency
686 of two. The model was further parameterized with monovalent binding affinities (K_D values) that
687 were experimentally determined here (as described in the above Methods; *Quantifying AbLec*
688 *binding and K_D*) and informed by the supporting literature. Affinities were parameterized as
689 follows: trastuzumab monovalent K_D = 11.2 nM and Siglec-7-Fc monovalent K_D = 200 μM[83,84].
690
691 The parameterized model was then used to fit the flow cytometry-based experimental binding
692 data for the apparent concentration ([C_{app}]) parameters that derive from the spatial, nearest-
693 neighbor proximity of pairs of targeted cell surface ligands/antigens. Model-derived estimates of
694 [C_{app}] for various designed topologies were interpreted as quantitative assessments of the relative
695 probability or favorability of a candidate therapeutic engaging with a particular cell surface in an
696 advantageous bivalent and high-avidity interaction.
697
698 *Expression and dye labeling of Siglec-Fc reagents*
699 Siglec-Fc decoy receptors were expressed in Expi293F cells that stably express human
700 formylglycine-generating enzyme for aldehyde tagging. Siglec-Fc constructs were expressed
701 according to the Expi293F manufacturer protocol (Thermo Fisher Scientific) and purified by
702 manual gravity column (BioRad) using protein A agarose (Fisher Scientific), as described for
703 antibodies above, with the modification that transfected cells, supernatant, and purified Siglec-
704 Fcs were stored in the dark. Siglecs were then buffer exchanged into acidic buffer, concentrated,
705 and conjugated with HIPS-azide as we previously described[16]. Siglec-Fc-azide was then buffer
706 exchanged into PBS, and 100x molar equivalents of DBCO-AF647 (Click Chemistry Tools, 1302-
707 1) in DMSO were added and the reaction was mixed at 500 rpm in the dark for 2 hours rt. Siglecs
708 were buffer exchanged into PBS by 6x centrifugation on Amicon columns (30 kDa MWCO) and

709 AF647 addition was confirmed by using a NanoDrop spectrophotometer at 650 nm for the AF647
710 dye (extinction coefficient 239,000) and at 280 nm for the protein (using extinction coefficients
711 calculated for each Siglec by Expasy).[85]
712
713 *Competitive binding assays*
714 HER2+ K562 cells were isolated from the cell culture supernatant, washed with 1xPBS, and
715 resuspended in blocking buffer. Cells were aliquoted for sialidase treatment with 100 nM *V.*
716 *cholerae* sialidase at 37 °C for 30 min in blocking buffer. 60,000 untreated or sialidase treated
717 cells were then distributed into wells of a 96-well V-bottom plate (Corning). Various concentrations
718 of trastuzumab or AbLecs were combined with 200 nM Siglec-7/9-Fc-AF647 or 0.3 µg/mL MEM-
719 59-AF647, added to the cells in equal volumes and incubated with cells for 2-3 h at 4 °C with
720 periodic pipet mixing. Cells were washed three times and resuspended in blocking buffer, pelleting
721 by centrifugation at 300 xg for 5 min at 4 °C between washes, and fluorescence was analyzed by
722 flow cytometry (BD LSR II). Gating was performed using FlowJo v.10.0 software (Tree Star) to
723 eliminate debris and isolate single cells. Mean fluorescence intensity (MFI) of the cell populations
724 were background subtracted and normalized to the MFI of cells stained with 200 nM Siglec-7/9-
725 Fc-AF647 without antibody or AbLecs from each experimental replicate.
726
727 *Cell growth and toxicity assays*
728 SK-BR-3 and HER2+ K562 cells were lifted with 2 mL trypsin for 5 min at 37 ºC, rinsed with 8 mL
729 normal growth media, pelleted by centrifugation at 300 *x g*, and resuspended in phenol-red-free
730 growth medium containing 50 nM Sytox green cell dead stain (Thermo Fisher Scientific) for
731 HER2+ K562 cells or 5 nM Sytox red dead cell stain (Thermo Fisher Scientific) for SK-BR-3 cells
732 to measure cytotoxicity. Cells were plated onto a flat-bottomed 96 well plate (10,000 cells per
733 well, 95 µL), then 5 µL of AbLec, Siglec, or antibody in PBS was added and mixed, followed by
734 centrifugation at 30 *x g* for 1 min. Images were acquired using an IncuCyte® S3 Live-Cell Analysis

735 System (Sartorius) every 2 h for 3 days. SK-BR-3 cells were analyzed by phase with segmentation
736 adjustment = 1, and a minimum area of 200 μm^2, cell death was quantified by red fluorescence
737 using a threshold of 0.3 RCU, with an edge sensitivity of -50 and areas between 50 and 1000
738 square microns. HER2+ K562 phase segmentation adjustment was 0.2, with no hole-fill and a
739 minimum area of 60 microns. Cell death was quantified by green fluorescence using a threshold
740 of 2 RCU, with an edge sensitivity of -45 and areas between 50 and 800 microns with eccentricity
741 and integrated intensities less than 0.95 and 40000, respectively.
742
743 *Isolation and differentiation of donor macrophages*
744 LRS chambers were obtained from anonymous healthy donors through the Stanford Blood
745 Center. PBMCs were isolated using Ficoll-Paque (Sigma-Aldrich) density gradient centrifugation.
746 Isolated PBMCs were extracted from the PBS/Ficoll interface, washed once with PBS, and
747 resuspended in serum-free RPMI. Monocytes were isolated by plating ~$1x10^8$ PBMCs in a T75
748 flask containing serum-free RPMI for 1-2 hours, followed by 3x washes with PBS +Ca +Mg to
749 remove non-adherent cells. The media was then replaced with IMDM with 10% Human AB Serum
750 (Gemini) and incubated for 7-9 days to induce macrophage differentiation prior to use in
751 phagocytosis or flow cytometry experiments.
752
753 *Phagocytosis assays*
754 Macrophages were washed with PBS and lifted by 30 min incubation at 37 ºC with 10 mL TrypLE
755 (Thermo Fisher Scientific). Macrophages were pelleted by centrifugation at 300 *x g* for 5 min and
756 resuspended in IncuCyte medium (phenol-red free RPMI + 10% HI FBS). Macrophages (10,000
757 cells, 100 µL) were added to a 96 well flat-bottom plate (Corning) and incubated in a humidified
758 incubator for 1 h at 37 ºC. Meanwhile, target cells were washed 1x with PBS, then treated with
759 1:80,000 diluted pHrodo red succinimydyl ester dye (Thermo Fisher Scientific) in PBS at 37 ºC
760 for 30 min, washed 1x with PBS and resuspended in IncuCyte medium. Finally, 10 µL of 20x

761 antibody or AbLec stocks in PBS were added to the macrophages, followed by addition of pHrodo
762 red-stained target cells (20,000 cells, 90 µL). Antibodies, Siglec-Fcs, and AbLecs were added at
763 25 nM, Siglec-7 and -9 blocking antibodies (1E8 and mAbA clones, respectively[20]; Creative
764 Biolabs) were used at 12.5-25 µg/mL, *V. cholerae* sialidase was used at 100 nM, and human IgG1
765 isotype antibody (BioXCell), rat IgG2a isotype antibody (BioXCell), and CD47 blocking antibody
766 (clone B6H12, BioXCell)[23] was added at 10 µg/mL unless otherwise noted. Cells were plated by
767 gentle centrifugation (50 *x g*, 2 min). Two images per well were acquired using an IncuCyte® S3
768 Live-Cell Analysis System (Sartorius) at 1 h intervals until the maximum signal was reached. The
769 quantification of pHrodo red fluorescence was empirically optimized for phagocytosis of each cell
770 line based on their background fluorescence and size. K562 and MDA-MB-231 cells were
771 analyzed with a threshold of 0.8, an edge sensitivity of -70, and the area was gated to between
772 100 and 2000 μm^2 with integrated intensities between 300 and 2000 RCU x μm^2 / image. HCC-
773 1954 were analyzed with a threshold of 1.5, an edge sensitivity of -45, and an area between 30
774 and 2000 μm^2. SK-BR-3 analysis had a threshold of 1, an edge sensitivity of -55, a minimum
775 integrated intensity of 60, and a maximum area and eccentricity 3000 and 0.96, respectively.
776 Ramos and Raji analysis used a threshold of 1.5, an edge sensitivity of -45, and areas between
777 100 and 2000 μm^2. The total red object integrated intensity (RCU × μm^2/Image) was quantified
778 for each image and the maximum total red object integrated intensity value is reported for each
779 treatment condition.
780
781 *Isolation of donor NK cells*
782 PBMCs were isolated from LRS chambers as described above, cryostocks were prepared at 2-
783 $4x10^7$ cells in 90% heat-inactivated FBS + 10% DMSO and stored in liquid nitrogen vapor until
784 use. The day prior to use stocks were thawed, NK cells were isolated using an EasySep NK
785 isolation kit (StemCell Technologies), and cells were cultured with 0.5 µg/mL recombinant IL-2

786 (BioLegend) in RPMI + 10% heat-inactivated FBS for 24 h before use in NK cell cytotoxicity or
787 flow cytometry experiments.
788
789 *NK cell killing assays*
790 Target cells were lifted with TrypLE (Thermo Fisher Scientific) and stained with CellTracker Deep
791 Red dye (Thermo Fisher Scientific) according to the manufacturer's protocol. NK cells and target
792 cells were mixed at an effector to target (E/T) ratio of 4:1 (SK-BR-3 cells) or 2:1 (K562 cells) and
793 Sytox Green (Thermo Fisher Scientific) was added at 100 nM. Antibodies, Siglec decoy receptors,
794 and AbLecs were added at 25 nM, Siglec-7 and -9 blocking antibodies (1E8 and mAbA clones,
795 respectively; Creative BioLabs)[20] were used at 12.5-25 µg/mL, CD16 blocking antibody (clone
796 3G8, BioLegend) was added at 10 µg/mL, and *V. cholerae* sialidase was used at 100 nM, unless
797 otherwise noted. After 5-6 h incubation at 37 °C, cell death was analyzed by flow cytometry by
798 selecting the CellTracker Deep Red^{+} cells and quantifying the percent dead as Sytox Green^{+} /
799 total CellTracker Deep Red^{+} cells. NK cytotoxicity index was then calculated as the ratio of dead
800 to alive cells in the assay: % dead / (100-% dead).
801
802 *Isolation of human PMNs*
803 Polymorphonuclear granulocytes (PMN) were isolated from peripheral blood of healthy donors by
804 density gradient centrifugation using either Polymorphprep® (Progen, Heidelberg, DE), as
805 previously described[86]. Isolated PMNs were >82% pure by flow cytometry.
806
807 *PMN cytotoxicity assays*
808 PMN-mediated cytotoxicity was analyzed in chromium-51 [^{51}Cr] release assays as previously
809 described[87]. AbLecs and antibodies were added at varying concentrations. The CD47 blocking
810 antibody hu5F9-IgG2σ was applied at 20 µg/ml. Effector cells and ^{51}Cr-labelled target cells were
811 added at a ratio of 40:1. After 3 h incubation at 37 °C, ^{51}Cr release was measured in counts per

812 minute (cpm) in a MikroBetaTrilux 1450 liquid scintillation and luminescence counter
813 (PerkinElmer, Rodgau Jügensheim, DE). Maximal ^{51}Cr release was achieved by addition of 2%
814 v/v Triton-X 100 solution, while basal ^{51}Cr release was measured in the absence of antibodies.
815 Specific tumor cell lysis in % was calculated as follows:

816 $$lysis\ [\%] = (experimental\ cpm - basal\ cpm)/(maximal\ cpm - basal\ cpm) \times 100$$

817

818 *Acquisition of IncuCyte images*

819 For phagocytosis and cytotoxicity assays, images were obtained over time using an Incucyte®
820 S3 Live-Cell Analysis System (Essen BioScience) within a Thermo Fisher Scientific tissue culture
821 incubator at maintained 37 °C with 5% CO_2. Data were acquired from a 10x objective lens in
822 phase contrast, a green fluorescence channel (ex: 460 ± 20, em: 524 ± 20, acquisition time:
823 300 ms), and from a red fluorescence channel (ex. 585 ± 20, em: 665 ± 40, acquisition time: 400
824 ms). Two images per well were acquired at intervals. Unless otherwise specified, all cells were
825 analyzed by Top-Hat segmentation with 100 µm radius, edge split on, hole fill: 0 μm^2.

826

827 *Mice*

828 WT C57BL/6 mice were purchased from The Jackson Laboratories and housed at Stanford
829 University. Experiments involving animals at Stanford University were approved by the
830 Administrative Panel on Lab Animal Care (APLAC) and carried out according to protocol number
831 31511. Stanford University vivaria are AAALAC-accredited. Husbandry is performed in
832 accordance with the Guide for the Care and Use of Laboratory Animals and the Public Health
833 Service Policy on Humane Care and Use of Laboratory Animals. SigE$^{-/-}$ and SigE$^{-/-}$ Sig7/9 mice
834 were developed previously[20] and were bred and maintained at the Comparative Bioscience
835 Center at The Rockefeller University. All experiments carried out at The Rockefeller University
836 were performed in compliance with federal laws and institutional guidelines and have been
837 approved by The Rockefeller University Institutional Animal Care and Use Committee. Animals

838 were housed under the following conditions: 12-h light/12-h dark cycle, ambient temperature of
839 20–22 °C and relative humidity of between 30 and 70%. All studies were performed on 8- to 12-
840 wk old age- and sex-matched female and male mice.
841
842 *Isolation of murine bone marrow*
843 Femurs, tibias, and fibias were collected from WT, SigE$^{-/-}$, and SigE$^{-/-}$ Sig7/9 mice. Bones were
844 sterilized with 96% ethanol and rinsed with PBS. Proximal and distal ends of bones were removed
845 and a 1 mL syringe with 26 gauge needle containing PBS was used to extract bone marrow and
846 resuspend until an approximately single cell suspension was achieved. The cell suspension was
847 then passed over a 70 µm filter, cells were pelleted at 200-250 xg for 5-10 min at rt, resuspended
848 at 5 x 10^6 cells/mL in heat-inactivated FBS + 10% DMSO, and stored in liquid nitrogen vapor until
849 use.
850
851 *Murine BMDM differentiation and activation assays*
852 Murine bone marrow cryostocks were thawed into 10 mL of warmed complete media (RPMI +
853 10% HI FBS + 1% penicillin/streptomycin), pelleted at 300 xg for 5 min rt, and plated in complete
854 media + 0.1 µg/mL M-CSF (PeproTech). After 3 and 5 days of incubation, the media was replaced
855 with complete media + 0.1 µg/mL M-CSF (PeproTech). BMDMs were allowed to differentiate in
856 refreshed media until use on days 7-9. For use in activation assays, BMDMs were lifted by 20 min
857 incubation at 37 ºC with 10 mL TrypLE (Thermo Fisher Scientific). BMDMs (10-15,000 cells, 100
858 µL) in complete media + 0.1 µg/mL M-CSF were added to a 96 well flat-bottom plate (Corning)
859 and incubated in a humidified incubator for 1 h at 37 ºC. Meanwhile, HER2+ B16D5 cells were
860 washed 1x with PBS, treated with 1:80,000 diluted pHrodo red succinimydyl ester dye (Thermo
861 Fisher Scientific) in PBS at 37 ºC for 30 min, washed 1x with PBS and resuspended in complete
862 media + 0.1 µg/mL M-CSF. Finally, 10 µL of 20x antibody or AbLec stocks in PBS were added to
863 the macrophages, followed by addition of pHrodo red-stained target cells (20,000 cells, 90 µL)

864 and BMDM/target cell co-cultures were incubated for 24 h. Following incubation, 100 μL
865 supernatant was collected and analyzed using a Cytometric Bead Array Mouse Inflammation Kit
866 (BD), according to the manufacturer's protocol.
867
868 *Isolation and activation of human T cells*
869 PBMCs were isolated from LRS chambers, cryostocks were prepared at 2-4x10^7 cells in 90%
870 heat-inactivated FBS + 10% DMSO, and stocks were stored in liquid nitrogen vapor until use, as
871 described above. Human T cells were isolated from thawed cryostocks using an EasySep CD3+
872 T cell isolation kit (StemCell Technologies). T cells were cultured at a 1:2 cell:bead ratio with
873 cultured αCD3/αCD28 activator beads (Thermo Fisher Scientific) and 50 ng/mL recombinant IL-
874 2 (BioLegend) in RPMI + 10% heat-inactivated FBS for 3 days before use.
875
876 *Statistical Analysis*
877 Statistical analysis was performed in Prism (version 9.0). For binding curves, one-site-specific
878 binding curves were used to calculate the dissociation constants of antibodies and AbLecs. In
879 binding assays, NK cell cytotoxicity experiments, phagocytosis experiments, and Siglec
880 expression analyses, ordinary one-way ANOVAs were performed with Tukey's multiple
881 comparison's test to compare treatment groups. All results were confirmed with multiple biological
882 replicates as indicated in the figure legends. All data were tested for outliers using GraphPad
883 Outlier Calculator (http://graphpad.com/quickcalcs/Grubbs1.cfm) and no outliers were identified.
884 In every instance ns indicates $p>0.05$, * indicates $p<0.05$, ** indicates $p<0.01$, *** indicates
885 $p<0.001$, and **** indicates $p<0.0001$.
886
887 **Acknowledgements**

J.C.S. acknowledges support from NIH/NCI F32 Postdoctoral Fellowship 1F32CA250324-01, American Cancer Society Postdoctoral Fellowship PF-20-143-01-LIB, and a Sarafan ChEM-H Postdocs at the Interface seed grant. S.W. is supported by funding from the Canadian Institutes of Health Research, the Natural Sciences and Engineering Research Council of Canada, the Cancer Research Society, the Canadian Cancer Society, the Arthritis Society of Canada, Health Research BC, and the Canadian Glycomics Network (GlycoNet). M.L. and T.V. acknowledge funding from the German Research Foundation (DFG KFO 5010 P6). M.A.G. acknowledges support from the National Science Foundation Graduate Research Fellowship and the Sarafan ChEM-H Chemistry/Biology Interface Predoctoral Training Program. N.M.R. acknowledges support from NIH grant K99GM147304. C.A.S. acknowledges support from NIH (R35 GM136309). C.R.B. acknowledges support from NIH (R01 GM058867-23, R01 CA227942, and U01 CA226051-02) and a Merck Research Labs Discovery Biologics SEEDS grant. Cell sorting/flow cytometry analysis for this project was performed using instruments in the Stanford Shared FACS Facility.

Author Contributions

J.C.S., M.A.G., S.P.W., and C.R.B. conceived the study. J.C.S., M.A.G., S.P.W., I.I.B., N.M.R., M.K.R, M.L., W.J.E., and B.B. designed and performed experiments and analyzed data. C.A.S., J.V.R., T.V., and C.R.B. directed research and aided in data analysis. J.C.S., M.A.G., and C.R.B. wrote the manuscript. All authors reviewed and/or revised the manuscript.

Conflict of Interest Statement

A patent application relating to antibody-decoy receptor chimeras has been filed by Stanford University (docket no. PCT/US2022/023166). Additionally, a patent for targeted cell surface editing mentioned in this work was filed by Stanford University (WO2018006034A1). J.C.S. and

913 C.R.B. are co-founders of Valora Therapeutics. C.R.B. is a co-founder and scientific advisory
914 board member of Firefly Bio, Lycia Therapeutics, Palleon Pharmaceuticals, Enable Bioscience,
915 Redwood Biosciences (a subsidiary of Catalent), OliLux Bio, Grace Science LLC, and InterVenn
916 Biosciences. All other authors have no conflicts of interest to declare.
917

918 Data and Materials Availability Statement

919 All primary data for main text and supplementary figures are available from the authors upon
920 reasonable request. Any unique materials presented in the manuscript may be available from the
921 authors upon reasonable request and through a materials transfer agreement.
922

923 References

924 1. Haslam, A. & Prasad, V. Estimation of the Percentage of US Patients With Cancer Who Are
925 Eligible for and Respond to Checkpoint Inhibitor Immunotherapy Drugs. *JAMA Netw Open* **2**,
926 e192535 (2019).

927 2. Schachter, J. *et al.* Pembrolizumab versus ipilimumab for advanced melanoma: final overall
928 survival results of a multicentre, randomised, open-label phase 3 study (KEYNOTE-006).
929 *Lancet* **390**, 1853–1862 (2017).

930 3. RodrÍguez, E., Schetters, S. T. T. & van Kooyk, Y. The tumour glyco-code as a novel immune
931 checkpoint for immunotherapy. *Nat. Rev. Immunol.* **18**, 204–211 (2018).

932 4. Rodrigues Mantuano, N., Natoli, M., Zippelius, A. & Läubli, H. Tumor-associated
933 carbohydrates and immunomodulatory lectins as targets for cancer immunotherapy. *J*
934 *Immunother Cancer* **8**, (2020).

935 5. Läubli, H. & Borsig, L. Altered Cell Adhesion and Glycosylation Promote Cancer Immune
936 Suppression and Metastasis. *Front. Immunol.* **10**, 2120 (2019).

937 6. Smith, B. A. H. & Bertozzi, C. R. The clinical impact of glycobiology: targeting selectins,
938 Siglecs and mammalian glycans. *Nat. Rev. Drug Discov.* **20**, 217–243 (2021).

939 7. Natoni, A., Macauley, M. S. & O'Dwyer, M. E. Targeting Selectins and Their Ligands in
940 Cancer. *Front. Oncol.* **6**, 93 (2016).

941 8. Liu, F.-T. & Rabinovich, G. A. Galectins as modulators of tumour progression. *Nat. Rev.*
942 *Cancer* **5**, 29–41 (2005).

943 9. Mariño, K. V., Cagnoni, A. J., Croci, D. O. & Rabinovich, G. A. Targeting galectin-driven
944 regulatory circuits in cancer and fibrosis. *Nat. Rev. Drug Discov.* **22**, 295–316 (2023).

945 10. Bandala-Sanchez, E. *et al.* T cell regulation mediated by interaction of soluble CD52 with the
946 inhibitory receptor Siglec-10. *Nat. Immunol.* **14**, 741–748 (2013).

947 11. Laubli, H. *et al.* Engagement of myelomonocytic Siglecs by tumor-associated ligands
948 modulates the innate immune response to cancer. *Proc. Natl. Acad. Sci. U. S. A.* **111**, 14211–
949 14216 (2014).

950 12. Xiao, H., Woods, E. C., Vukojicic, P. & Bertozzi, C. R. Precision glycocalyx editing as a
951 strategy for cancer immunotherapy. *Proc. Natl. Acad. Sci. U. S. A.* **113**, 10304–10309 (2016).

952 13. Stanczak, M. A. *et al.* Self-associated molecular patterns mediate cancer immune evasion
953 by engaging Siglecs on T cells. *J. Clin. Invest.* **128**, 4912–4923 (2018).

954 14. Wang, J. *et al.* Siglec-15 as an immune suppressor and potential target for normalization
955 cancer immunotherapy. *Nat. Med.* **25**, 656–666 (2019).

956 15. Barkal, A. A. *et al.* CD24 signalling through macrophage Siglec-10 is a target for cancer
957 immunotherapy. *Nature* **572**, 392–396 (2019).

958 16. Gray, M. A. *et al.* Targeted glycan degradation potentiates the anticancer immune response
959 in vivo. *Nat. Chem. Biol.* **16**, 1376–1384 (2020).

960 17. Wisnovsky, S. *et al.* Genome-wide CRISPR screens reveal a specific ligand for the glycan-
961 binding immune checkpoint receptor Siglec-7. *Proc. Natl. Acad. Sci. U. S. A.* **118**, (2021).

962 18. Rodriguez, E. *et al.* Sialic acids in pancreatic cancer cells drive tumour-associated
963 macrophage differentiation via the Siglec receptors Siglec-7 and Siglec-9. *Nat. Commun.* **12**,
964 1270 (2021).

965 19. Haas, Q. *et al.* Siglec-9 Regulates an Effector Memory CD8+ T-cell Subset That Congregates
966 in the Melanoma Tumor Microenvironment. *Cancer Immunol Res* **7**, 707–718 (2019).

967 20. Ibarlucea-Benitez, I., Weitzenfeld, P., Smith, P. & Ravetch, J. V. Siglecs-7/9 function as
968 inhibitory immune checkpoints in vivo and can be targeted to enhance therapeutic antitumor
969 immunity. *Proc. Natl. Acad. Sci. U. S. A.* **118**, (2021).

970 21. Haas, Q. *et al.* Siglec-7 represents a glyco-immune checkpoint for non-exhausted effector
971 memory CD8+ T cells with high functional and metabolic capacities. *Front. Immunol.* **13**,
972 996746 (2022).

973 22. Stanczak, M. A. *et al.* Targeting cancer glycosylation repolarizes tumor-associated
974 macrophages allowing effective immune checkpoint blockade. *Sci. Transl. Med.* **14**,
975 eabj1270 (2022).

976 23. Theruvath, J. *et al.* Anti-GD2 synergizes with CD47 blockade to mediate tumor eradication.
977 *Nat. Med.* **28**, 333–344 (2022).

978 24. Schmassmann, P. *et al.* Targeting the Siglec-sialic acid axis promotes antitumor immune
979 responses in preclinical models of glioblastoma. *Sci. Transl. Med.* **15**, eadf5302 (2023).

980 25. Egan, H. *et al.* Targeting stromal cell sialylation reverses T cell-mediated immunosuppression
981 in the tumor microenvironment. *Cell Rep.* **42**, 112475 (2023).

982 26. Lustig, M. *et al.* Disruption of the sialic acid/Siglec-9 axis improves antibody-mediated
983 neutrophil cytotoxicity towards tumor cells. *Front. Immunol.* **14**, 1178817 (2023).

984 27. Mei, Y. *et al.* Siglec-9 acts as an immune-checkpoint molecule on macrophages in
985 glioblastoma, restricting T-cell priming and immunotherapy response. *Nat Cancer* (2023)
986 doi:10.1038/s43018-023-00598-9.

987 28. Sterner, E., Flanagan, N. & Gildersleeve, J. C. Perspectives on Anti-Glycan Antibodies
988 Gleaned from Development of a Community Resource Database. *ACS Chem. Biol.* **11**,
989 1773–1783 (2016).

29. Smith, B. A. H. *et al.* MYC-driven synthesis of Siglec ligands is a glycoimmune checkpoint. *Proc. Natl. Acad. Sci. U. S. A.* **120**, e2215376120 (2023).

30. Varki, A. & Angata, T. Siglecs--the major subfamily of I-type lectins. *Glycobiology* **16**, 1r–27r (2006).

31. Pedram, K. *et al.* Design of a mucin-selective protease for targeted degradation of cancer-associated mucins. *Nat. Biotechnol.* (2023) doi:10.1038/s41587-023-01840-6.

32. Filipovic, A. *et al.* 482 Phase1/2 study of an anti-galectin-9 antibody, LYT-200, in patients with metastatic solid tumors. *J Immunother Cancer* **9**, (2021).

33. Shum, E. *et al.* 490 Clinical benefit through Siglec-15 targeting with NC318 antibody in subjects with Siglec-15 positive advanced solid tumors. *J Immunother Cancer* **9**, (2021).

34. Luke, J. J. *et al.* Abstract CT034: GLIMMER-01: initial results from a phase 1 dose escalation trial of a first-in-class bi-sialidase (E-602) in solid tumors. *Cancer Res.* **83**, CT034–CT034 (2023).

35. Dimitriou, F. *et al.* Frequency, Treatment and Outcome of Immune-Related Toxicities in Patients with Immune-Checkpoint Inhibitors for Advanced Melanoma: Results from an Institutional Database Analysis. *Cancers* **13**, (2021).

36. Perez, E. A. *et al.* Incidence of adverse events with therapies targeting HER2-positive metastatic breast cancer: a literature review. *Breast Cancer Res. Treat.* **194**, 1–11 (2022).

37. Sakuishi, K. *et al.* Targeting Tim-3 and PD-1 pathways to reverse T cell exhaustion and restore anti-tumor immunity. *J. Exp. Med.* **207**, 2187–2194 (2010).

38. Yang, R. *et al.* Galectin-9 interacts with PD-1 and TIM-3 to regulate T cell death and is a target for cancer immunotherapy. *Nat. Commun.* **12**, 1–17 (2021).

39. Merchant, A. M. *et al.* An efficient route to human bispecific IgG. *Nat. Biotechnol.* **16**, 677–681 (1998).

40. Delaveris, C. S., Chiu, S. H., Riley, N. M. & Bertozzi, C. R. Modulation of immune cell reactivity with cis-binding Siglec agonists. *Proc. Natl. Acad. Sci. U. S. A.* **118**, (2021).

41. Errington, W. J., Bruncsics, B. & Sarkar, C. A. Mechanisms of noncanonical binding dynamics in multivalent protein–protein interactions. *Proceedings of the National Academy of Sciences* **116**, 25659–25667 (2019).

42. Bruncsics, B., Errington, W. J. & Sarkar, C. A. MVsim is a toolset for quantifying and designing multivalent interactions. *Nat. Commun.* **13**, 1–13 (2022).

43. McCord, K. A. *et al.* Dissecting the Ability of Siglecs To Antagonize Fcγ Receptors. *ACS Cent. Sci.* (2024) doi:10.1021/acscentsci.3c00969.

44. Wang, Y. *et al.* Specificity of mouse and human Fcgamma receptors and their polymorphic variants for IgG subclasses of different species. *Eur. J. Immunol.* **52**, 753–759 (2022).

45. Sharma, P. & Allison, J. P. Immune checkpoint targeting in cancer therapy: toward combination strategies with curative potential. *Cell* **161**, 205–214 (2015).

46. Garcia-Manero, G. *et al.* Magrolimab + azacitidine versus azacitidine + placebo in untreated higher risk (HR) myelodysplastic syndrome (MDS): The phase 3, randomized, ENHANCE study. *J. Clin. Orthod.* **39**, TPS7055–TPS7055 (2021).

47. Wolchok, J. D. *et al.* Overall Survival with Combined Nivolumab and Ipilimumab in Advanced Melanoma. *N. Engl. J. Med.* **377**, 1345–1356 (2017).

1032 48. Hodi, F. S. *et al.* Improved survival with ipilimumab in patients with metastatic melanoma. *N.*
1033 *Engl. J. Med.* **363**, 711–723 (2010).

1034 49. Overman, M. J. *et al.* Durable Clinical Benefit With Nivolumab Plus Ipilimumab in DNA
1035 Mismatch Repair-Deficient/Microsatellite Instability-High Metastatic Colorectal Cancer. *J.*
1036 *Clin. Oncol.* **36**, 773–779 (2018).

1037 50. Le, D. T. *et al.* Phase II Open-Label Study of Pembrolizumab in Treatment-Refractory,
1038 Microsatellite Instability-High/Mismatch Repair-Deficient Metastatic Colorectal Cancer:
1039 KEYNOTE-164. *J. Clin. Oncol.* **38**, 11–19 (2020).

1040 51. Motzer, R. J. *et al.* Nivolumab plus Ipilimumab versus Sunitinib in Advanced Renal-Cell
1041 Carcinoma. *N. Engl. J. Med.* **378**, 1277–1290 (2018).

1042 52. Choueiri, T. K. *et al.* Nivolumab plus Cabozantinib versus Sunitinib for Advanced Renal-Cell
1043 Carcinoma. *N. Engl. J. Med.* **384**, 829–841 (2021).

1044 53. Rini, B. I. *et al.* Pembrolizumab plus Axitinib versus Sunitinib for Advanced Renal-Cell
1045 Carcinoma. *N. Engl. J. Med.* **380**, 1116–1127 (2019).

1046 54. Reck, M. *et al.* Pembrolizumab versus Chemotherapy for PD-L1–Positive Non–Small-Cell
1047 Lung Cancer. *N. Engl. J. Med.* **375**, 1823–1833 (2016).

1048 55. Cascone, T. *et al.* Neoadjuvant nivolumab or nivolumab plus ipilimumab in operable non-
1049 small cell lung cancer: the phase 2 randomized NEOSTAR trial. *Nat. Med.* **27**, 504–514
1050 (2021).

1051 56. Jin, H.-T. *et al.* Cooperation of Tim-3 and PD-1 in CD8 T-cell exhaustion during chronic viral
1052 infection. *Proc. Natl. Acad. Sci. U. S. A.* **107**, 14733–14738 (2010).

1053 57. Borate, U. *et al.* Phase Ib Study of the Anti-TIM-3 Antibody MBG453 in Combination with
1054 Decitabine in Patients with High-Risk Myelodysplastic Syndrome (MDS) and Acute Myeloid
1055 Leukemia (AML). *Blood* **134**, 570–570 (2019).

1056 58. Acharya, N., Sabatos-Peyton, C. & Anderson, A. C. Tim-3 finds its place in the cancer
1057 immunotherapy landscape. *J Immunother Cancer* **8**, (2020).

1058 59. Curigliano, G. *et al.* Phase I/Ib Clinical Trial of Sabatolimab, an Anti-TIM-3 Antibody, Alone
1059 and in Combination with Spartalizumab, an Anti-PD-1 Antibody, in Advanced Solid Tumors.
1060 *Clin. Cancer Res.* **27**, 3620–3629 (2021).

1061 60. Kaufman, H. L. *et al.* Avelumab in patients with chemotherapy-refractory metastatic Merkel
1062 cell carcinoma: a multicentre, single-group, open-label, phase 2 trial. *Lancet Oncol.* **17**,
1063 1374–1385 (2016).

1064 61. Motzer, R. J. *et al.* Avelumab plus Axitinib versus Sunitinib for Advanced Renal-Cell
1065 Carcinoma. *N. Engl. J. Med.* **380**, 1103–1115 (2019).

1066 62. Powles, T. *et al.* Avelumab Maintenance Therapy for Advanced or Metastatic Urothelial
1067 Carcinoma. *N. Engl. J. Med.* **383**, 1218–1230 (2020).

1068 63. Tarantino, P. *et al.* HER2-Low Breast Cancer: Pathological and Clinical Landscape. *J. Clin.*
1069 *Orthod.* **38**, 1951–1962 (2020).

1070 64. Schettini, F. *et al.* Clinical, pathological, and PAM50 gene expression features of HER2-low
1071 breast cancer. *npj Breast Cancer* **7**, 1–13 (2021).

1072 65. Jamal-Hanjani, M. *et al.* Tracking the Evolution of Non-Small-Cell Lung Cancer. *N. Engl. J.*
1073 *Med.* **376**, 2109–2121 (2017).

1074 66. Walker, A. J. *et al.* Tumor Antigen and Receptor Densities Regulate Efficacy of a Chimeric
1075 Antigen Receptor Targeting Anaplastic Lymphoma Kinase. *Mol. Ther.* **25**, 2189–2201 (2017).

1076 67. Majzner, R. G. & Mackall, C. L. Tumor Antigen Escape from CAR T-cell Therapy. *Cancer*
1077 *Discov.* **8**, 1219–1226 (2018).

1078 68. Upton, R. *et al.* Combining CD47 blockade with trastuzumab eliminates HER2-positive breast
1079 cancer cells and overcomes trastuzumab tolerance. *Proc. Natl. Acad. Sci. U. S. A.* **118**,
1080 (2021).

1081 69. Fernandes, R. A. *et al.* Immune receptor inhibition through enforced phosphatase
1082 recruitment. *Nature* **586**, 779–784 (2020).

1083 70. Lippert, A. H. *et al.* Antibody agonists trigger immune receptor signaling through local
1084 exclusion of receptor-type protein tyrosine phosphatases. *Immunity* **57**, 256-270.e10 (2024).

1085 71. Juszczynski, P. *et al.* The AP1-dependent secretion of galectin-1 by Reed Sternberg cells
1086 fosters immune privilege in classical Hodgkin lymphoma. *Proc. Natl. Acad. Sci. U. S. A.* **104**,
1087 13134–13139 (2007).

1088 72. Ilarregui, J. M. *et al.* Tolerogenic signals delivered by dendritic cells to T cells through a
1089 galectin-1-driven immunoregulatory circuit involving interleukin 27 and interleukin 10. *Nat.*
1090 *Immunol.* **10**, 981–991 (2009).

1091 73. Dardalhon, V. *et al.* Tim-3/galectin-9 pathway: regulation of Th1 immunity through promotion
1092 of CD11b+Ly-6G+ myeloid cells. *J. Immunol.* **185**, 1383–1392 (2010).

1093 74. Zhou, Q. *et al.* Coexpression of Tim-3 and PD-1 identifies a CD8+ T-cell exhaustion
1094 phenotype in mice with disseminated acute myelogenous leukemia. *Blood* **117**, 4501–4510
1095 (2011).

1096 75. Kouo, T. *et al.* Galectin-3 Shapes Antitumor Immune Responses by Suppressing CD8+ T
1097 Cells via LAG-3 and Inhibiting Expansion of Plasmacytoid Dendritic Cells. *Cancer Immunol*
1098 *Res* **3**, 412–423 (2015).

1099 76. Daley, D. *et al.* Dectin 1 activation on macrophages by galectin 9 promotes pancreatic
1100 carcinoma and peritumoral immune tolerance. *Nat. Med.* **23**, 556–567 (2017).

1101 77. Tiraboschi, C. *et al.* Combining inhibition of galectin-3 with and before a therapeutic
1102 vaccination is critical for the prostate-tumor-free outcome. *J Immunother Cancer* **8**, (2020).

1103 78. Sturgill, E. R. *et al.* Galectin-3 inhibition with belapectin combined with anti-OX40 therapy
1104 reprograms the tumor microenvironment to favor anti-tumor immunity. *Oncoimmunology* **10**,
1105 1892265 (2021).

1106 79. Cagnoni, A. J. *et al.* Galectin-1 fosters an immunosuppressive microenvironment in colorectal
1107 cancer by reprogramming CD8+ regulatory T cells. *Proc. Natl. Acad. Sci. U. S. A.* **118**, (2021).

1108 80. Li, Y. M. *et al.* Upregulation of CXCR4 is essential for HER2-mediated tumor metastasis.
1109 *Cancer Cell* **6**, (2004).

1110 81. Bern, M., Kil, Y. J. & Becker, C. Byonic: Advanced peptide and protein identification software.
1111 *Current Protocols in Bioinformatics* (2012) doi:10.1002/0471250953.bi1320s40.

1112 82. Elias, J. E. & Gygi, S. P. Target-decoy search strategy for increased confidence in large-
1113 scale protein identifications by mass spectrometry. *Nature Methods* **4**, (2007).

1114 83. Yamaji, T., Teranishi, T., Alphey, M. S., Crocker, P. R. & Hashimoto, Y. A small region of the
1115 natural killer cell receptor, Siglec-7, is responsible for its preferred binding to alpha 2,8-disialyl

1116 and branched alpha 2,6-sialyl residues. A comparison with Siglec-9. *J. Biol. Chem.* **277**,
1117 6324–6332 (2002).

1118 84. Attrill, H. *et al.* Siglec-7 Undergoes a Major Conformational Change When Complexed with
1119 the α(2,8)-Disialylganglioside GT1b*. *J. Biol. Chem.* **281**, 32774–32783 (2006).

1120 85. Gasteiger, E. *et al.* ExPASy: the proteomics server for in-depth protein knowledge and
1121 analysis. *Nucleic Acids Research* **31**, 3784–3788 (2003).

1122 86. Derer, S. *et al.* Increasing FcγRIIa affinity of an FcγRIII-optimized anti-EGFR antibody
1123 restores neutrophil-mediated cytotoxicity. *MAbs* **6**, 409–421 (2014).

1124 87. Lohse, S. *et al.* An Anti-EGFR IgA That Displays Improved Pharmacokinetics and Myeloid
1125 Effector Cell Engagement In Vivo. *Cancer Res.* **76**, 403–417 (2016).

1126 88. Kulkarni, R. U., Wang, C. L. & Bertozzi, C. R. Analyzing nested experimental designs-A user-
1127 friendly resampling method to determine experimental significance. *PLoS Comput. Biol.* **18**,
1128 e1010061 (2022).